

THE SEARCH FOR THE QUARK-GLUON PLASMA

John W. Harris

Physics Department, Yale University, New Haven, Connecticut 06520, and Lawrence
 Berkeley Laboratory, University of California, Berkeley, California 94720

Berndt Müller

Department of Physics, Duke University, Durham, North Carolina 27708

KEY WORDS: QCD, deconfinement, chiral symmetry restoration, high-density nuclear matter,
 relativistic heavy-ion collisions, AGS, SPS, RHIC, LHC, quark matter, phase
 transitions

ABSTRACT

We provide an overview of the present understanding of the transition from hadrons to a quark-gluon plasma, its signatures, and the experimental results so far. We discuss results of numerical simulations of the lattice gauge theory and critically evaluate the various observables that have been proposed as signatures of the QCD phase transition. We place the existing data from relativistic heavy-ion experiments at the Brookhaven Alternating Gradient Synchrotron (AGS) and CERN Super Proton Synchrotron (SPS) into perspective and provide an overview of the techniques and strategies that will be employed in the search for the quark-gluon plasma at heavy-ion colliders, such as the Relativistic Heavy-Ion Collider (RHIC) and the Large Hadron Collider (LHC).

CONTENTS

1. INTRODUCTION	72
1.1 The QCD Phase Transition	72
1.2 Abnormal Nuclear Matter	74
2. THEORETICAL GUIDANCE AND EXPECTATIONS	75
2.1 Lattice Gauge Theory	75
2.2 Thermal Perturbation Theory	75
2.3 Dynamical Models of Relativistic Heavy-Ion Collisions	77
3. PLASMA SIGNATURES	79

3.1	<i>Kinematic Probes</i>	79
3.2	<i>Electromagnetic Probes</i>	80
3.3	<i>Probes of Deconfinement</i>	82
3.4	<i>Probes of Chiral Symmetry Restoration</i>	83
3.5	<i>Hard QCD Probes</i>	84
4.	EXPERIMENT	85
4.1	<i>Experimental Conditions</i>	85
4.2	<i>Present Relativistic Heavy-ion Accelerators</i>	85
4.3	<i>Heavy-ion Colliders</i>	86
4.4	<i>Detector Components</i>	87
4.5	<i>Detector Systems and Measurements</i>	88
5.	CURRENT UNDERSTANDING OF DATA	89
5.1	<i>Baryon and Energy Stopping</i>	89
5.2	<i>Thermal Equilibration—Temperatures and Flow</i>	91
5.3	<i>Chemical Equilibration—Strangeness Production</i>	92
5.4	<i>Two-Particle Correlations</i>	93
5.5	<i>Resonance Matter</i>	94
5.6	<i>Virtual and Real Photons</i>	94
5.7	<i>J/ψ Suppression</i>	95
6.	FUTURE MEASUREMENTS	95
6.1	<i>Kinematic Probes</i>	95
6.2	<i>Electromagnetic Probes</i>	96
6.3	<i>Probes of Deconfinement</i>	97
6.4	<i>Probes of Chiral Symmetry Restoration</i>	97
6.5	<i>Other Probes</i>	98
7.	SUMMARY	98

1. INTRODUCTION

1.1 *The QCD Phase Transition*

Strongly interacting matter is described at the fundamental level by the interaction of quarks through the exchange of gluons. This non-Abelian gauge theory, called quantum chromodynamics (QCD), exhibits a number of remarkable features. (a) At short distances or large momenta q , the effective coupling constant $\alpha_s(q^2)$ decreases logarithmically, i.e. quarks and gluons appear to be weakly coupled. (b) At large distances or small momenta, the effective coupling becomes strong, resulting in the phenomena of quark confinement (the technical term used to describe the observation that quarks do not occur isolated in nature but only in hadronic bound states as mesons and baryons) and chiral symmetry breaking (an expression of the fact that quarks confined in hadrons do not appear as nearly massless constituents but are endowed with a dynamically generated mass of several hundred MeV). (c) At low energies, the QCD vacuum is characterized by nonvanishing expectation values of certain operators, usually called vacuum condensates, which encode the nonperturbative physical properties of the QCD vacuum. Most important for this discussion are the quark condensate $\langle \bar{\psi}\psi \rangle \approx (235 \text{ MeV})^3$, and the gluon condensate $\langle \alpha_s G_{\mu\nu} G^{\mu\nu} \rangle \approx (500 \text{ MeV})^4$ (1).

The quark condensate describes the density of quark-antiquark pairs found in the QCD vacuum, which is the source of chiral symmetry breaking. The gluon condensate measures the density of gluon pairs in the QCD vacuum and is a manifestation of the breaking of scale invariance of QCD by quantum effects.

It is not uncommon in nature that spontaneously broken symmetries are restored at high temperature through phase transitions. Well-known examples are ferromagnetism, superconductivity, and the transition from solid to liquid. More closely connected to our subject is nuclear matter at low temperatures, which has a dense liquid phase that transforms into a dilute gaseous phase at $T > 5$ MeV. Evidence for this phase transition has recently been observed in nuclear collisions at intermediate energies (2).

As the temperature increases in QCD, the interactions among quanta occur at ever shorter distances, governed by weak coupling, whereas the long-range interactions become dynamically screened. This picture is supported by finite-temperature perturbation theory, which shows that the effective coupling constant $\alpha_s(T)$ falls logarithmically with increasing temperature (3), and also by more general arguments (4). As a consequence, nuclear matter at very high temperature exhibits neither confinement nor chiral symmetry breaking. This new phase of QCD is called the quark-gluon plasma.

Because there exist order parameters, such as the quark condensate, that vanish at high temperature,¹ there are good reasons to expect that the transition between the low-temperature and high-temperature phases of QCD is not smooth but exhibits a discontinuity, i.e. a phase transition. The order of the chiral phase transition is believed to be quite sensitive to the number of light, dynamical quark flavors. Universality arguments (6, 7) predict a second-order phase transition for two massless flavors and a first-order transition for three massless flavors. Numerical simulations of lattice gauge theory (see Section 2.1) have established that the transition temperature lies in the range 150 ± 10 MeV at vanishing net quark density.

According to the standard cosmological model (8), the temperature of the cosmic background radiation exceeded 200 MeV during the first 10 μ s after the Big Bang. The early universe was hence filled with a quark-gluon plasma rather than with hadrons. Thus, physical processes occurring during this very early period can be described in terms of quark and gluon transition amplitudes rather than hadronic amplitudes. This facilitates reliable calculations of transport

¹Two technical notes: This statement neglects the effect of finite current quark masses; and the situation is somewhat unusual for the deconfinement transition in the pure non-Abelian gauge theory. Here, the $Z(3)$ center symmetry is broken spontaneously at high temperature, allowing free quarks to exist, whereas it is manifest in the QCD vacuum, causing quark confinement (5).

processes, such as baryon number violating processes during the electroweak phase transition.

Chiral symmetry is also expected to be restored at high baryon density even at zero temperature. Many model studies of this phenomenon have been performed, yielding critical densities $4\rho_0 < \rho_c < 10\rho_0$, where ρ_0 denotes the ground state density of nuclear matter. Because ab initio calculations based on lattice QCD are not yet feasible, the uncertainty of ρ_c remains large. One expects a smooth connection between the high- T and high- ρ phase transitions, giving rise to a continuous phase boundary $T_c(\rho)$. For $T < T_c(\rho)$, the effective description of strongly interacting matter at low momenta is in terms of hadronic degrees of freedom (baryons and mesons), whereas for $T > T_c(\rho)$ the effective degrees of freedom at low momenta carry the quantum numbers of quarks and gluons.

It is important to recognize that this difference is only discernible at momenta below the chiral symmetry breaking scale $q_{\text{CSB}}^2 \approx (4\pi f_\pi)^2 \approx 1 \text{ GeV}^2$. For processes involving momentum transfers above that scale, light quarks are effectively massless and deconfined in either phase. An effective description above q_{CSB}^2 must, therefore, always be based on the elementary degrees of freedom (quarks and gluons). Hence, experimental signatures for the change in the structure of strongly interacting matter must be sensitive to the dynamics of the low-energy degrees of freedom of QCD. Quarks and gluons are already known to provide the correct description for momenta $q^2 \gg q_{\text{CSB}}^2$. Quark-gluon plasma signals must probe the momentum range $q^2 < q_{\text{CSB}}^2$ and show that, within this range, current quarks and gluons remain effective degrees of freedom when $T > T_c(\rho)$.

1.2 *Abnormal Nuclear Matter*

It is speculated that additional phases of baryon-rich nuclear matter exist: pion condensates (9, 10), density isomers (11), nuclear matter with a large strangeness content (12–16), and others. Of these, kaon condensates and strange quark matter appear to be the best established. Some models of hadron structure predict that strange quark matter is the true ground state of nuclear matter (17–20). In other models, strange quark matter may be unstable against weak decay but stable under strong interactions. The basic argument for an increased stability of strange matter is that the Fermi energy can be lowered significantly by distributing the given baryon number over three, rather than only two, quark flavors. But there is a price: the higher current quark mass of the strange quark and, possibly, the destruction of the color-singlet structure of baryons. The energy balance for these different aspects is delicate; hence, reliable predictions are impossible without a better knowledge of baryon structure in the framework of QCD.

Mechanisms for the separation of strange quark matter have been conceived in the environment of the early universe (14) as well as in relativistic heavy-ion reactions (21–24). Although rather strong astrophysical limits on the density of strange quark matter “nuggets” (strangelets) exist in our universe (25), the search for strange quark matter produced in heavy-ion collisions has only just begun. The experimental signature for light multi-strange nuclei would be an abnormally low charge-to-mass ratio.

2. THEORETICAL GUIDANCE AND EXPECTATIONS

2.1 *Lattice Gauge Theory*

Lattice gauge theory (26, 27) allows for a potentially exact, nonperturbative numerical calculation of observables in QCD. Improvements of the original algorithms, together with significant increases in computing power due to parallel processing, have permitted fairly reliable evaluations of the thermodynamic averages of many interesting quantities, which can be extrapolated to the infinite volume limit. State-of-the-art simulations of finite temperature lattice gauge theory employ lattices with spatial size 12^3 and with four points in the Euclidean time direction (28). Simulations of pure SU(3) gauge theory without quarks are possible on much larger lattices, such as $32^3 \times 12$ (29).

The simulations without dynamical quarks clearly exhibit a first-order phase transition at a temperature $T_c \approx 260$ MeV. Below T_c , the free energy of an isolated quark is infinite; above T_c it is finite. Hence, quarks are not confined in the high-temperature phase. The quark condensate $\langle \bar{\psi}\psi \rangle$ shows a strong drop over the same temperature range (see Figure 1), indicating that deconfinement and restoration of chiral symmetry go hand-in-hand.

Simulations of lattice QCD with dynamical quarks have not yet overcome the limitations due to finite lattice size. Present results indicate a smooth crossover between phases for $N_f = 2$ light quark flavors and a first-order phase transition for $N_f \geq 3$. Figure 2 shows recent results (at $N_f = 2$) for the energy density ϵ and pressure P as a function of temperature. $\epsilon(T)/T^4$ shows a dramatic rise. The thermal change in the pressure P is much smoother, causing a large difference between $3P$ and ϵ in the transition region. The large value of $(3P - \epsilon)$ arises naturally as a consequence of the rapid rise of the number of active degrees of freedom, i.e. a sudden increase of the entropy density near the phase transition (29a). The effect can also be described assuming that the propagating degrees of freedom have an effective thermal mass (30, 31).

2.2 *Thermal Perturbation Theory*

Many of the properties of the quark-gluon plasma far above T_c can be calculated in the framework of thermal perturbation theory. Neglecting current quark

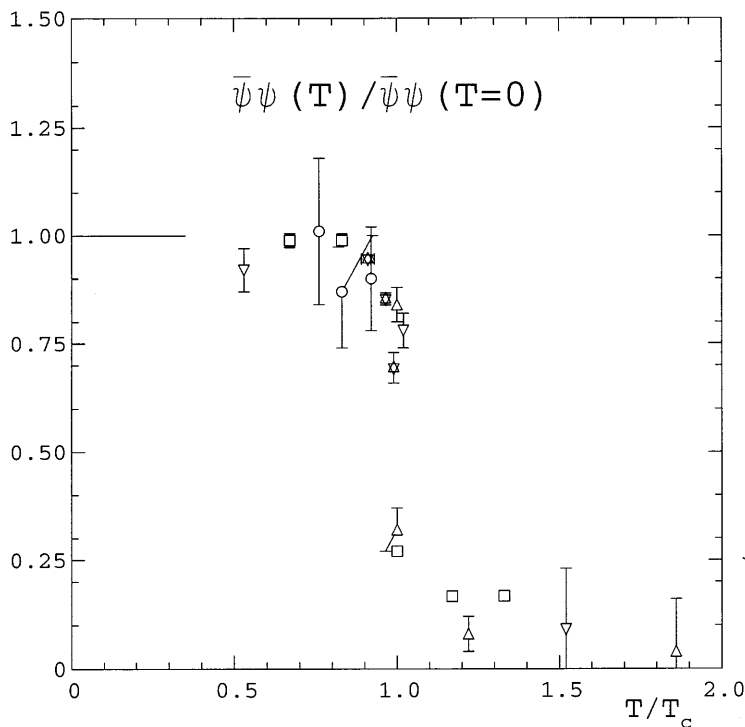


Figure 1 Quark condensate $\langle \bar{\psi} \psi \rangle$ as a function of temperature T , normalized to the vacuum quark condensate, from lattice calculations with and without dynamical quarks. The condensate drops rapidly to (almost) zero at the critical temperature T_c . (From Reference 29.)

masses, the equation of state up to the order of $g^2 = 4\pi\alpha_s$ is given by (32–34)

$$\begin{aligned} \epsilon = & \left(1 - \frac{15}{16\pi^2}g^2\right)\frac{8\pi^2}{15}T^4 + N_f\left(1 - \frac{50}{84\pi^2}g^2\right)\frac{7\pi^2}{10}T^4 \\ & + \sum_f \left(1 - \frac{2}{4\pi^2}g^2\right)\frac{3}{\pi^2}\mu_f^2\left(\pi^2T^2 + \frac{1}{2}\mu_f^2\right), \end{aligned} \quad 1.$$

where f denotes the quark flavors and μ_f denotes the quark chemical potential of each flavor. Higher-order corrections have been calculated for $\mu_f = 0$, up to the order of g^5 (35). Various arguments can be made that α_s should be taken at an effective momentum scale on the order of $2\pi T$, corresponding to $\alpha_s \approx 0.3$ at the critical temperature, or $g \approx 2$.

Additional insight into the properties of the interacting quark-gluon plasma is obtained by considering the dispersion relations of small perturbations carrying the quantum numbers of quarks or gluons (36, 37). These excitations govern the dissipation mechanisms in the quark-gluon plasma. For gluonic excitations, one obtains two different modes, with transverse and longitudinal polarization, respectively. Soft gluonic excitations, also called plasmons, carry an effective mass on the order of $gT/\sqrt{3}$. The plasmon mode is strongly damped. In the limit $k \rightarrow 0$, the plasmon decay width is $\Gamma \approx \frac{1}{2}g^2T$, which provides an estimate for the thermalization time of a quark-gluon plasma (38). The static longitudinal gluon propagator is screened with screening mass $m_E \approx gT$, whereas the transverse propagator remains unscreened (lack of magnetic screening). Lattice simulations indicate a localization of static color-magnetic fields at the momentum scale g^2T . The screening of color-electric fields lies at the origin of the deconfinement of quarks at high temperature.

2.3 Dynamical Models of Relativistic Heavy-Ion Collisions

2.3.1 PARTON CASCADES Relativistic heavy-ion collisions are the most promising tool for creating a quark-gluon plasma in the laboratory. QCD predicts

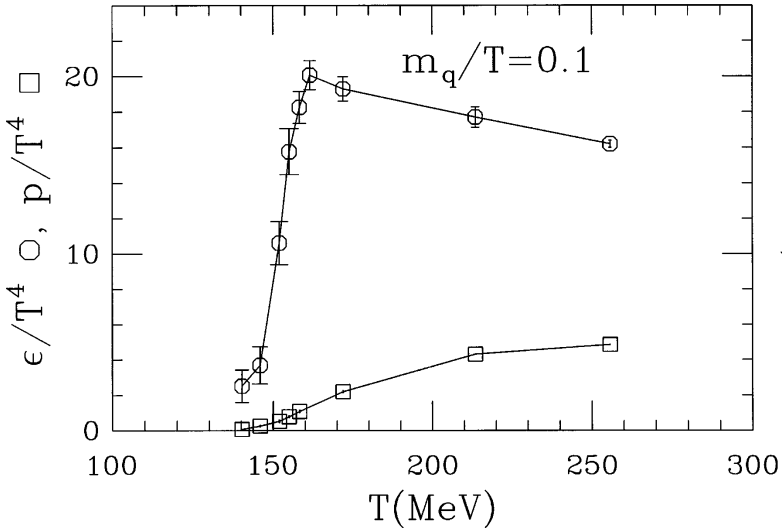


Figure 2 Energy density ϵ (upper curve) and pressure p (lower curve) obtained from a numerical evaluation of QCD “on the lattice” with two light flavors of quarks. ϵ and p are divided by T^4 to exhibit the sudden rise in the number of thermally excited degrees of freedom at the critical temperature $T_c \approx 150$ MeV due to liberation of color and chiral symmetry restoration. (From Reference 28.)

that the energy density at midrapidity grows like $A^{2/3}$, where A is the nuclear mass (39, 40), but at most logarithmically with the center-of-mass energy. To reach temperatures far above T_c , the initial kinetic energy of the nuclei must be rapidly thermalized on a time scale on the order of 1 fm/c. Early ideas about the mechanism of energy deposition were based either on the inside-outside cascade model of parton scattering (41) or on the breaking of color flux tubes (42, 43). More recently, detailed microscopic models have been constructed (44–46) that permit the study of the energy deposition process, in space-time as well as in momentum space, within the framework of perturbative QCD. These models are based on the concept that the colliding nuclei can be decomposed into their parton substructure. The perturbative interactions among these partons can then be followed until thermalization. One finds that partonic cascades account for at least half the expected energy deposition at RHIC and for an even larger fraction in the energy range of the LHC (47).

Parton cascade models predict a very rapid thermalization of the deposited energy. This is caused by a combination of radiative energy degradation and kinematic separation of partons with different rapidities. The transverse momentum distribution of initially scattered partons is already to a high degree exponential if radiative processes are taken into account. The subsequent expansion causes the local longitudinal momentum distribution of partons to coincide with the transverse distribution after a time approximately equal to the mean time between parton interactions. The models predict that thermalization occurs on a proper time scale of 0.3–0.5 fm/c at RHIC energies (47).

Due to the large cross sections and higher branching probabilities of gluons, the thermalized parton plasma is initially gluon rich and rather depleted of quarks (48). Chemical equilibration of the parton plasma proceeds over a time of several fm/c in most scenarios (49, 50), but may be faster if higher-order QCD processes are important (51).

Another interesting issue concerns the inhomogeneity of initial conditions. Partonic cascades can lead to a rather uneven energy deposition, because of cross-section fluctuations. Hot spots caused by strongly inelastic parton scatterings could lead to observable, nonstatistical fluctuations in the final hadron distribution (52).

2.3.2 HYDRODYNAMIC MODELS After (local) momentum equilibration, further evolution of the quark-gluon plasma to its final dissolution can be described in the framework of relativistic hydrodynamics. According to the results of parton cascade models, the initial conditions for this evolution in the central rapidity region are boost invariant to a large degree, as anticipated by Bjorken (53). Assuming purely longitudinal expansion, the temperature then falls as $\tau^{-1/3}$, where τ is the local proper time. Cooling is substantially enhanced by the transverse expansion generated by the high internal pressure of the plasma

when the initial temperature is significantly above T_c . Typical estimates of the plasma lifetime are 4 fm/c, after which a mixed quark-hadron phase is formed in a first-order phase transition (54). Because of transverse expansion, however, even the mixed phase decays on a time scale of 10 fm/c. Where the pressure is minimal, the lifetime of the mixed phase could be longer if the plasma were formed at the critical temperature without initial collective flow (55, 56). This may occur at energies far below those accessible at RHIC—likely between the current AGS and SPS energies—in a regime where our understanding of the thermalization mechanism is rather limited. A long-lived ($\gg 10$ fm/c) mixed phase could be detected by its effect on two-particle correlations (57, 58).

The hydrodynamic approach becomes invalid when the typical distance between particles exceeds the mean free path. This happens shortly after the quark-hadron phase transition, when the temperature falls below 120–130 MeV (59, 60). Because various hadrons have different mean free paths, the freeze-out for baryon-rich matter is differential with K^+ -mesons freezing out first, followed by nucleons, K^- , and finally pions.

3. PLASMA SIGNATURES

Experimental investigations of the quark-gluon plasma require the identification of appropriate experimental tools for observing its formation and for studying its properties. One serious problem is that the size and lifetime of the plasma are expected to be small, at most a few fermi in diameter and perhaps 5–10 fm/c in duration. Furthermore, signals of the quark-gluon plasma compete with backgrounds emitted from the hot hadronic gas phase that follows the hadronization of the plasma and are modified by final-state interactions in the hadronic phase. In spite of this, a wealth of ideas has been proposed in the past decade as to how the identification and investigation of the short-lived quark-gluon plasma phase could be accomplished. It is beyond the scope of this review to present a comprehensive survey of quark-gluon plasma signatures. We therefore concentrate on the most promising ones. More details can be found elsewhere (61–64).

3.1 *Kinematic Probes*

The basic concept behind kinematic probes is the determination of the energy density ϵ , pressure P , and entropy density s of superdense hadronic matter as a function of the temperature T and the baryochemical potential μ_B . One seeks to observe a rapid rise in the effective number of degrees of freedom, as expressed by the ratios ϵ/T^4 or s/T^3 , over a small temperature range.

Observables related to the variables T , s , and ϵ are customarily identified with the average transverse momentum $\langle p_T \rangle$, the hadron rapidity distribution dN/dy , and the transverse energy dE_T/dy , respectively (65). In principle, one

can invert the ϵ - T diagram of Figure 2 and plot $\langle p_T \rangle$ as a function of dN/dy or dE_T/dy . If a rapid change in the effective number of degrees of freedom occurs, one expects an S-shaped curve, whose essential characteristic feature is the saturation of $\langle p_T \rangle$ during the persistence of a mixed phase, continuing into a second rise when the structural change from color singlet to colored constituents has been completed.

The high pressure of the quark-gluon plasma leads to the formation of a collective outward flow during the expansion of the dense matter. Detailed numerical studies in the context of the hydrodynamical model have shown that this characteristic transverse flow of particles is rather weak in realistic models (66, 67). The strength of this signal can be enhanced by studying the full transverse momentum distributions of hadrons (67a), or heavier hadrons such as baryons (68). The transverse flow signal would be enhanced by the formation of a detonation wave during the hadronization transition (69, 75–77).

Identical-particle interferometry, e.g. $\pi\pi$, KK , or NN correlations, yields information on the reaction geometry and provides important information about the space-time dynamics of nuclear collisions. By studying the two-particle correlation function along various directions in phase space, it is possible to obtain measurements of the transverse and longitudinal size, of the lifetime, and of flow patterns of the hadronic fireball at the moment when it breaks up into separate hadrons (57, 58, 77a). Recent theoretical work has shown the importance of the finite lifetime of the fireball (78), of flow patterns (79, 79a), and of shadowing effects (80). Because interferometric size determinations will be possible on an event-by-event basis for collisions of heavy nuclei at the SPS, RHIC, and LHC, the correlation of global parameters like $\langle p_T \rangle$ and dN/dy with the fireball geometry can be performed on individual collision events.

3.2 *Electromagnetic Probes*

Photons and lepton pairs provide probes of the interior of the quark-gluon plasma during the earliest and hottest phase of the evolution of the fireball because they are not affected by final-state interactions. Unfortunately, these probes have rather small yields and must compete with relatively large backgrounds from hadronic processes, especially electromagnetic hadron decays.

In the hadronic phase, the electromagnetic response function is dominated by the ρ^0 resonance at 770 MeV. On the other hand, perturbative QCD predicts a broad continuous spectrum above twice the thermal quark mass $m_q = gT/\sqrt{6}$ in the high-temperature phase. Below 100 MeV, collective modes are predicted to exist in both phases.

3.2.1 LEPTON PAIRS Many of the original calculations on lepton pairs as probes of the quark-gluon plasma (81–88) concentrated on invariant masses

in the range below the ρ -meson mass. With an improved understanding of the collision dynamics and the hadronic backgrounds (89, 90), it has since become clear (91) that lepton pairs from the quark-gluon plasma can probably only be identified for invariant masses above 1–1.5 GeV. At the high-mass end, the yield of Drell-Yan pairs from first nucleon-nucleon collisions exceeds the thermal dilepton yield.

Recent progress in understanding the mechanisms of thermalization has revealed that the yield of high-mass dileptons critically depends on, and provides a measure of, the thermalization time (92). Lepton pairs from the equilibrating quark-gluon plasma may dominate over the Drell-Yan background up to masses in the range 5–10 GeV, as predicted by the parton cascade (93) and other models of the early equilibration phase of the nuclear collision (94, 95). If this turns out to be true, the early thermal evolution of the quark-gluon phase can be traced in a rather model independent way (96). Dileptons from charm decay are predicted to yield a substantial contribution to the total dilepton spectrum and could, because of their different kinematics, provide a measure of the total charm yield (97). This yield may be enhanced as a result of rescattering of gluonic partons (98, 99), if the direct background (100, 100a) is sufficiently well understood.

Lepton pairs from hadronic sources in the invariant-mass range between 0.5 and 1 GeV are important signals of the dense hadronic matter formed in nuclear collisions (101, 102). They provide exclusive information about possible in-medium modifications of hadronic properties, especially of the ρ -meson, at high density (103, 104). Another strategy for using the leptonic ρ -meson decay as a probe of the hadronic phase of the fireball is based on the idea that the ρ peak is expected to grow strongly relative to the ω peak in the lepton pair mass spectrum, if the fireball lives substantially longer than 2 fm/c. Because of the short average lifetime of the ρ -meson, the ρ/ω ratio can, therefore, serve as a fast “clock” for the fireball lifetime (105).

3.2.2 DIRECT PHOTONS In contrast to the lepton-pair spectrum, the hadronic radiation spectrum is not concentrated in a single narrow resonance. The dominant source of photons from the thermal hadron gas is the $\pi\rho \rightarrow \gamma\rho$ reaction (106), to which the broad a_1 resonance may be an important contribution (107). In the quark phase, the gluon-photon Compton process $gq \rightarrow \gamma q$ dominates. Infrared singularities occurring in perturbation theory are softened by screening effects (106, 108). The result is that a hadron gas and a quark-gluon plasma in the vicinity of the critical temperature T_c emit photon spectra of roughly equal intensity and similar spectral shape.

However, a clear signal of photons from the quark-gluon plasma could be visible for transverse momenta p_T in the range 2–5 GeV/c if a very hot plasma

is formed initially (96, 109, 110). The photon spectrum in the p_T range 1–2 GeV/ c is mostly emitted from the mixed phase. Transverse flow effects make the separation of the contributions from the different phases more difficult (112) and destroy the correlation between the slope of the photon spectrum in the intermediate p_T range and the temperature of the mixed phase (113).

3.3 *Probes of Deconfinement*

3.3.1 QUARKONIUM SUPPRESSION The suppression of J/ψ production (114) in a quark-gluon plasma occurs because a $c\bar{c}$ pair formed by fusion of two gluons from the colliding nuclei cannot bind inside the quark-gluon plasma (115). Lattice simulations of SU(3) gauge theory (116, 117) show that this condition should be satisfied already slightly above the deconfinement temperature. The screening length appears to be even shorter when dynamical fermions are included in the lattice simulations (118, 119). Excited states of the $(c\bar{c})$ system, such as ψ' and χ_c , are more easily dissociated and should disappear as soon as the temperature exceeds T_c . For the heavier $\Upsilon(b\bar{b})$ system similar considerations apply, although shorter screening lengths are required than for the charmonium states (120). The dissociation temperature of the Υ ground state is predicted to be around $2.5 T_c$, that of the larger Υ' state only slightly above T_c .

Owing to its finite size, the formation of a $(c\bar{c})$ bound state requires a time on the order of 1 fm/ c (121–123). The J/ψ may still survive, if it escapes from the region of high density and temperature before the $c\bar{c}$ pair has been spatially separated by more than the size of the bound state (114). This will happen either if the quark-gluon plasma cools very fast, or if the J/ψ has sufficiently high transverse momentum (124–127). On the other hand, the charmonium may also be destroyed by sufficiently energetic collisions with comoving hadrons, leading to dissociation into a pair of D -mesons (128, 129). Dissociation via quark exchange with mesons composed of light quarks, such as the ρ -meson, has been estimated in a nonrelativistic quark model (130) to reach several millibarns. Similar values are obtained if J/ψ production is fed by a large fraction of easily absorbed color-octet $(c\bar{c})$ states (130a, 131). Additional effects that can contribute to J/ψ suppression even in hadron-nucleus interactions are nuclear shadowing of soft gluons, initial-state scattering of partons resulting in a widened transverse momentum distribution, and final-state absorption on nucleons (132–134). Suppression mechanisms based on interactions with comoving particles generally predict that the ψ' state should be more strongly suppressed than the J/ψ (120, 135). This holds equally for a quark-gluon plasma as for a comoving thermalized gas of hadrons.

3.3.2 STRANGENESS ENHANCEMENT The production of hadrons containing strange quarks is normally suppressed in hadronic reactions compared with

the production of hadrons containing only up and down valence quarks (136). This suppression increases with growing strangeness content of the produced hadrons. When a quark-gluon plasma is formed, the production of hadrons carrying strange quarks is expected to be saturated because the strange quark content of the plasma is rapidly equilibrated by $s\bar{s}$ pair production in interactions of two gluons (137). As a result, the yield of multi-strange baryons and strange antibaryons is predicted to be strongly enhanced in the presence of a quark-gluon plasma (138, 139).

In addition, the relative abundances of the various strange particle species (mesons, strange and multi-strange baryons, and their antiparticles) allow the determination of relative strangeness equilibrium, saturation in the overall strangeness content (γ_s), and strangeness neutrality in a thermochemical approach (140). These ratios can be calculated assuming either a hadron gas scenario or a quark-gluon plasma scenario, and a comparison can be made of the values extracted from the models in the two scenarios in conjunction with other thermodynamic variables of the system, such as the temperature T , the baryo-chemical potential μ_B , and the entropy (141, 142).

Because strange hadrons interact strongly, their final-state interactions must be modeled in considerable detail before firm predictions about strange-hadron yields are possible. Theoretical studies (139, 143) have shown that an enhanced strangeness content can neither be destroyed nor generated by interactions during the breakup phase. Fragmentation processes during the hadronization phase transition can contribute significantly to the final abundances of strange hadrons (144), but this does not invalidate the usefulness of strangeness enhancement as a plasma signature.

3.4 *Probes of Chiral Symmetry Restoration*

3.4.1 DISORIENTED CHIRAL CONDENSATES The temporary restoration of chiral symmetry in nuclear collisions may result in the formation of domains of disoriented chiral condensate (DCC) (145). This term describes a coherent excitation of the pion field corresponding to a local misalignment of the chiral order parameter $\langle\bar{\psi}\psi\rangle$. Such domains would decay into neutral and charged pions, favoring pion charge ratios N_{π^0}/N_π substantially different from one third. This could explain why final states with a large fraction of charged pions over neutral pions, observed in Centauro events (146), can occur with significant probability (147, 148).

A DCC can be described as a nonlinear pion wave (149, 150). Such a wave can be excited by the growth of local instabilities during the transition from the chirally restored high-temperature phase of QCD to the low-temperature phase, in which chiral symmetry is broken (145, 151). The growth of long wavelength

modes in the chiral order parameter then occurs quite naturally if the transition proceeds out of equilibrium (152).

This picture has been partially confirmed in numerical calculations based on the linear sigma model (153–155). As the coherence length is inversely proportional to the growth rate of the instabilities (156, 157), larger domains of coherently excited pion fields may emerge if the chiral order parameter is somewhat, but not far, away from its equilibrium value, as is likely to occur in a relativistic heavy-ion reaction (158). Initial deviations from isospin neutrality do not necessarily destroy the usefulness of this probe (159). The observation of pion charge ratios significantly different from $1/3$, or nonzero charge correlations (160), would therefore be a direct signature of the chiral phase transition.

Domains of disoriented chiral condensate may also contribute to antibaryon production through the formation of topological defects in the chiral order parameter (161, 162). Such defects can arise at the intersection of chiral domain walls, which carry baryon number and eventually evolve into baryons and antibaryons, possibly leaving a signature of the chiral phase transition in regions of phase space that are normally baryon poor (163).

3.4.2 MEDIUM EFFECTS ON HADRON PROPERTIES The widths and positions of the ρ , ω , and ϕ peaks in the lepton-pair spectrum are sensitive to medium-induced changes of the hadronic mass spectrum, especially to the possible drop of vector meson masses preceding the chiral symmetry restoration transition (70–74, 164–168). In the absence of high baryon density, modifications of the peak positions are predicted to be small except in the immediate vicinity of the phase transition, whereas the increase in the width of the ϕ -meson due to collision broadening is substantial (169). This could serve as a measure of the density of the mixed phase (111). A change in the K-meson mass also would affect the width of the ϕ meson (170, 171). A double ϕ peak in the lepton pair spectrum would be indicative of a long-lived mixed phase (172).

3.5 *Hard QCD Probes*

The color structure of QCD matter can be probed by its effects on the propagation of a fast parton (173, 174). The mechanisms are similar to those responsible for the electromagnetic energy loss of a fast charged particle in matter: Energy may be lost either by excitation of the penetrated medium or by radiation.

The connection between energy loss of a quark and the color-dielectric polarizability of the medium can be established in a way analogous to the theory of electromagnetic energy loss (175–177). Although radiation is an efficient energy-loss mechanism for relativistic particles, it is strongly suppressed in a dense medium, because the charged particle often rescatters before the radiation has been emitted (178). The QCD analog of this effect has recently been

analyzed comprehensively (179, 180). By adding the two contributions, the stopping power of a fully established quark-gluon plasma is predicted to be higher than that of hadronic matter.

A quark or gluon jet propagating through a dense medium will not only lose energy, it will also be deflected. This effect destroys the coplanarity of the two jets from a hard parton-parton scattering with the incident beam axis (181–182a). The angular deflection of the jets also results in an azimuthal asymmetry. The presence of a quark-gluon plasma is also predicted to enhance the emission of jet pairs with small azimuthal opening angles (183). The sharp increase in the acoplanarity of di-jet events in proton-nucleus interactions recently observed at Fermilab (184) indicates that the interpretation of these signals is complicated by reinteraction. Another proposal is to use the reconstructed total transverse momentum vector of all jets to measure the momentum distribution in the dense matter (184a).

4. EXPERIMENT

4.1 *Experimental Conditions*

The techniques used in experiments studying relativistic nucleus-nucleus collisions are similar to those used in high-energy physics experiments. The primary difference is that the particle multiplicities and the backgrounds for various processes differ between the nuclear and the particle physics environments. For central collisions, with impact parameters near zero, the particle multiplicities scale approximately as the mass of the colliding system and, therefore, with nuclear masses around 200, can be a factor of 200 times higher in collisions of heavy nuclei compared to that in collisions between protons at the same energy. The multiplicities scale weakly as a function of energy with $dn/dy(y_{\text{cm}}) \sim \ln(\sqrt{s})$. Likewise, the combinatorial backgrounds underlying processes such as Drell-Yan production, particle and resonance decays, and photon production increase more than linearly with (and usually as the square root of) increasing primary particle multiplicities, complicating reconstruction of these signals.

4.2 *Present Relativistic Heavy-ion Accelerators*

Currently, two research facilities for relativistic heavy-ion experiments are focused on dense hadronic matter and signatures of quark-gluon plasma formation: the Brookhaven Alternating Gradient Synchrotron (AGS) and the CERN Super Proton Synchrotron (SPS), both in operation with heavy ions since 1986. (Two other relativistic heavy-ion facilities at somewhat lower energies, which focus on properties of the nuclear equation of state, are the GSI-Darmstadt SIS accelerator, and the JINR-Dubna Nucleotron.) Experiments utilize nuclear

beams ranging, at the AGS and SPS, respectively, from protons to gold, with momenta up to $29(Z/A)$ GeV/ c , and from protons to lead, with momenta up to $400(Z/A)$ GeV/ c , where Z is the element number and A is the atomic mass number of the nuclear beam. These correspond to center-of-mass (c.m.) energies per nucleon pair of 4.84 GeV for Au + Au collisions at the AGS and 17.2 GeV for Pb + Pb collisions at the SPS. Simply scaling the particle multiplicities measured in pp interactions by A , the charged particle multiplicity density at midrapidity for these systems is approximately 150 per unit rapidity at the AGS and 270 per unit rapidity at the SPS.

In these experiments, the collisions occur with a target in the laboratory frame, in contrast to colliding beams. The products are, thus, focused toward forward angles in the laboratory. For example, midrapidity ($\theta_{\text{c.m.}} = 90^\circ$) corresponds to $\theta_{\text{lab}} \leq 20^\circ$ and $\theta_{\text{lab}} \leq 5.5^\circ$ at the AGS and SPS, respectively, for the majority of particles emitted with less than 1 GeV/ c transverse momentum. To study particles emitted in the midrapidity region, the experiments require compact, highly segmented detectors placed in the forward regions downstream from the target. The particle momenta are relatively high due to the Lorentz boost of the c.m. into the laboratory frame, making particle identification via ionization-energy loss and time-of-flight more difficult. Particles at midrapidity have momenta in the relativistic rise region; thus, energy-loss measurements require larger numbers of samples along tracks (185) as well as exceptional track-separation capabilities.

4.3 *Heavy-ion Colliders*

There are two colliders being planned that will focus on acceleration of heavy-ions to ultra-relativistic energies. The Relativistic Heavy-ion Collider (RHIC) (186), presently under construction at Brookhaven National Laboratory in New York, is a dedicated heavy-ion collider planned for experiments in 1999. RHIC will accelerate and collide ions from protons to heavy nuclei, such as Au at c.m. energies up to 500 GeV for protons and 200 GeV per nucleon pair for Au nuclei. The luminosity for Au + Au will be $2 \times 10^{26} \text{ cm}^{-2} \text{ s}^{-1}$. Near head-on collisions of Au + Au at RHIC are expected to produce from 500 to 1500 charged particles per unit pseudorapidity at midrapidity in a single collision. Large detector systems are being constructed (187) to analyze the products of these interactions for evidence of formation of a quark-gluon plasma and a possible chiral phase transition.

Heavy-ion physics research (188) will also be an integral part of the program for the LHC, to be constructed at CERN, the European Centre for Nuclear Physics, in Geneva, Switzerland. For Pb nuclei, the c.m. energies at the LHC will be 5.4 TeV per nucleon pair with luminosities of $10^{27} \text{ cm}^{-2} \text{ s}^{-1}$. Predictions for the charged-particle densities at the LHC for near head-on collisions of Pb

+ Pb range from 2000 to 8000 per unit pseudorapidity. The large uncertainty in these numbers arises primarily from the present lack of information on the distributions of soft gluons in nuclei (189).

4.4 *Detector Components*

The types of detectors anticipated for use in the collider experiments can be divided into four categories: detectors for charged-particle tracking; calorimeters for energy measurements; detectors for particle identification; and photon detectors. In contrast to the high-energy physics environment, at the heavy-ion colliders (a) the p_T of the particles of interest is typically lower, (b) the luminosities are considerably lower, allowing the use of slower detectors and readout times, and (c) the particle multiplicities are considerably higher, requiring finer segmentation of detectors and larger event sizes.

Tracking detectors utilize the ionization of a charged particle traversing a medium in order to determine its trajectory. For tracking near the primary collision region within 5–10 cm, where particle densities approach $100\text{--}1000\text{ cm}^{-2}$, silicon detectors (pixels, strips, drift) (190) with excellent position ($20\text{ }\mu$) and double-track ($200\text{ }\mu$) resolution are used. Measurements close to the primary interaction are particularly important for detecting decays of short-lived strange and charm particles, of extreme importance in quark-gluon plasma searches. For large area tracking away from the interaction region and at more moderate particle densities of $\sim 1\text{ cm}^{-2}$, time-projection chambers and other types of tracking detectors are used (191).

The calorimeters used at the heavy-ion colliders will be of two basic types. Conventional sampling calorimeters (193) can be used for electromagnetic and hadronic energy determination and for measurements of jets. Highly segmented calorimeters can be used, in addition to the above measurements, to measure high-energy particles and photons. New types of calorimeters (194) with fine segmentation and various types of readout have recently been designed and tested for use in the high track density environments at heavy-ion colliders.

Particle identification of charged particles can be accomplished by using ionization energy loss, Cerenkov radiation, transition radiation, or time-of-flight techniques. At higher momenta, combinations of these techniques are sometimes necessary for best results, especially when measuring over a wide range of p_T over which any single technique may not be applicable.

Highly segmented photon detectors will be utilized for the measurement of photon radiation. Detectors from new types of materials have been developed [see, for example, (195)] for higher efficiencies and with smaller Molière radius to be able to improve performance and to more finely segment photon detector systems.

4.5 *Detector Systems and Measurements*

There are various types of detector systems that will be utilized at the heavy-ion colliders. For illustration, we briefly point out three and describe the measurements they allow.

4.5.1 HADRON SPECTROMETERS Hadron spectrometers utilize tracking detectors, detectors for particle identification, and magnetic fields to determine particle types and their momenta. Such spectrometers measure momentum (and rapidity) distributions for a large variety of identified particles, including decays of particles and resonances. For larger acceptances, particle correlations can be measured. The PHOBOS (196) and BRAHMS (197) experiments planned for RHIC are examples of these. For very large acceptances, approaching complete solid-angle coverage, measurements of single-event observables can be performed. The STAR experiment (198) under construction for RHIC and the ALICE experiment (199) planned for the LHC are examples. Such measurements will be unique to the high-multiplicity, heavy-ion experiments. Some examples of single-event observables are the strangeness content; temperatures of pions and kaons derived from the spectra or mean transverse momenta; event shapes and source sizes; and energy, momentum, and particle-number fluctuations as a function of emission direction. The purpose is to link these observables to thermodynamic variables and other dynamical properties of the evolving system and, thus, gain information on the dynamical evolution and state of the system. An additional aspect of large acceptance spectrometers is the ability to measure jets.

4.5.2 LEPTON PAIR SPECTROMETERS Lepton pair spectrometers typically measure e^+e^- , $\mu^+\mu^-$, and $e\mu$. They focus primarily on the lepton-pair mass spectrum over the entire mass range available, leptonic decays of hadronic resonances (including the J/ψ and higher mass resonances when possible), and on the Drell-Yan background. Here again, a magnetic field is utilized for momentum measurements along with arrays of detectors for tracking and for particle identification. The PHENIX experiment (200) under construction for RHIC is an example. Besides using various techniques to distinguish particle pairs from the decays in the primary heavy-ion interaction, it is also important to differentiate between particle pairs produced in the primary interaction and those produced in secondary processes away from the primary vertex. Because the yields of higher-mass pairs are low and because the branching ratios for the electromagnetic decays to e^+e^- , $\mu^+\mu^-$, and $e\mu$ are small ($1/137^2$) compared with hadronic decay modes, suppression of hadronic background sources relative to the electromagnetic signals (by factors of 10^{-4} or better) requires excellent tracking as well as particle identification using various combinations of detectors.

4.5.3 PHOTON SPECTROMETERS Highly segmented photon spectrometers seek to measure direct photon radiation from the various phases of matter formed in heavy-ion collisions. Such measurements require very elaborate detection systems to suppress the photons from neutral pion decay and electron conversion in order to measure the direct photons. The extraction of weak direct photon signals from the background requires a detailed and careful analysis of systematic errors and subtraction of the combinatorial background, and an understanding of the sensitivity to the various decay backgrounds. In addition to the efficiencies, the multiplicity dependence of the identification of the various particles creating the backgrounds must be understood.

5. CURRENT UNDERSTANDING OF DATA

The quark-gluon plasma has yet to be uniquely observed or identified. There are, however, experimental observations that require for their description more than our present understanding of the standard model of hadronic interactions. Some require modifications to existing microscopic models, due primarily to the high-density environment of these reactions; others are more easily described by models incorporating deconfined quarks and gluons. In this section, we place into perspective the present understanding of the data and review briefly new features that affect this understanding. Emphasis is given to the QGP signatures and those observations that require more than hadronic interactions for their description.

The status of the experimental results at these c.m. energies, $s^{1/2} = 5\text{--}20$ GeV, was last summarized in this publication in 1992 (201). Since that time, there has been significant progress in understanding the interactions of nuclei at high energy. This is the result of recent sophisticated measurements, availability of heavy nuclear beams, accumulation of systematic data, and improved theoretical-model calculations.

5.1 *Baryon and Energy Stopping*

The nuclear stopping power is a measure of the degree to which the energy of relative motion of two incident nuclei is transferred into other degrees of freedom. The amount of nuclear stopping determines basic parameters, such as energy in and volume of the interaction region and, thus, energy density. It governs the reaction dynamics and the extent to which conditions are favorable for the formation of a deconfined phase. Experiments determine the stopping power of colliding nuclei from (a) the redistribution of the incident protons into proton final-state rapidity distributions, (b) measurements of the energy remaining in the forward-going baryons that carry the initial energy into the reaction, and (c) measurements of the transverse energy distributions that represent the energy transformed into produced particles and their kinetic motion.

Many systems have been studied at the AGS and the SPS to determine the nuclear stopping power. The rapidity distributions for protons from pp interactions (202) and peripheral nucleus-nucleus interactions at the AGS (203, 204) and SPS (205) energies are peaked forward and backward in the c.m. frame, near the projectile and target rapidities, exhibiting a small degree of stopping. For central collisions of two intermediate mass nuclei ($A \sim 30$), the proton rapidity distributions spread over the entire rapidity space with broad peaks approximately half-way between the target/projectile and the c.m. rapidities, thereby exhibiting a fairly large amount of stopping at both energies (203–205). The distributions for the heavy systems (mass $A \sim 200$) at both energies exhibit a pileup of matter at midrapidity (206, 207). The heavier systems are more efficient at stopping the incoming matter, and thus, higher energy densities are expected to be reached when colliding these heavier nuclei.

The measured rapidity distributions of protons and produced particles at the AGS energy can be reproduced by the ARC cascade model (208). This model describes the nuclear reaction as a sequential binary cascade of interactions among known hadrons, neglecting all medium effects on the hadron-hadron cross sections. This is not sufficient at the higher SPS energies, especially for the proton distributions. The rapidity distributions of protons from central collisions of 160 A-GeV/c Pb + Pb exhibit a considerably higher degree of stopping than was predicted by models based on binary hadron interactions with free-space cross sections, such as HIJING (44), VENUS (209) and FRITIOF (210). There apparently exist important mechanisms for the transfer of baryon number that are not incorporated in binary cascade models. To successfully describe the measured rapidity distributions of baryons at SPS energy, cascade models have had to incorporate novel reaction mechanisms involving multihadronic intermediate states, such as color ropes in RQMD (211) or multiquark clusters in VENUS (212). The presence of these effects must be viewed as a result of the high density. They show that nuclear collisions at SPS energies require a description that goes beyond conventional hadronic interaction physics.

The transverse energy E_T distributions have also been measured to determine the degree of nuclear stopping in central heavy-ion collisions at the AGS and SPS. Measurements of E_T at the AGS (213) have shown that the E_T increases fifty percent more rapidly, in going from Si + Al to Au + Au, than was predicted from an independent nucleon-nucleon interaction model. An interpretation of this increase in a microscopic model (ARC) (208) infers a considerable increase in the baryon density, up to ten times normal nuclear density, and an accompanying large increase in the volume of high density matter when going from Si + Al to Au + Au at the AGS (214). At the SPS, measurements of E_T in central collisions of 160 A-GeV/c Pb + Pb (215) exhibit a large amount

of energy transfer into particle production. The accompanying energy density was estimated to be 3 GeV/fm^3 , similar to the results obtained for 200 A-GeV/c S + Au central collisions (216) but over a larger volume.

Overall nuclear stopping is found to be large in collisions of heavy systems at both the AGS and SPS energies. There is a significant buildup of baryon and energy density over a large volume and considerable energy transfer from the initial relative motion into particle production, suggesting that conditions may be favorable for thermal and chemical equilibrium.

5.2 *Thermal Equilibration—Temperatures and Flow*

The application of thermodynamic concepts to multiparticle production has a long history. Strictly speaking, the concept of temperature applies only to systems in thermal equilibrium with a heat bath. In high-energy interactions, the kinetic energy of the longitudinal motion, along the beam axis, serves as an energy reservoir. Thermalization is normally only thought to occur in the transverse degrees of freedom. The transverse momentum distributions measured in nucleus-nucleus collisions reflect conditions at the time when interactions cease (freeze out). Because of the large reinteraction cross sections for hadrons, the observed distributions do not reflect earlier conditions, as in a hot and dense deconfined phase, when chemical and thermal equilibrium may have been established. It, therefore, is not feasible to extract a temperature from the slopes of hadron spectra and relate to it an observable of the high-density phase, such as entropy or energy density. Prior to this, a better understanding of the effects on the spectra of final-state interactions and collective flow is necessary.

A discussion of the systematics of the slopes of the spectra of various particles and colliding systems measured at the AGS and SPS has been presented elsewhere (201). The momentum spectra for the produced light particles are not thermal and have significant deviations both at low p_T ($\leq 0.25 \text{ GeV}/c$) and at high p_T ($\geq 1.0 \text{ GeV}/c$). A collective nuclear flow component [originally observed in relativistic nuclear interactions at the Bevalac (217)] has been measured in azimuthal energy distributions at the AGS (218). This evidence for collective flow clearly underlines the need for a better understanding and description of the particle spectra. It is necessary to incorporate collective flow into models and to be able to subtract its effects before any extraction of temperatures from spectra. The measured transverse momentum and transverse mass distributions are consistent with a thermal description at freeze-out only if additional collective radial flow and feeding from higher-lying resonances are taken into consideration. (Note that these effects cannot be explicitly separated in the spectra alone.)

Data measured at the AGS for 14.6 A-GeV/c Si + Au (203) are compatible with thermal distributions, including transverse flow with temperatures $120 <$

$T < 140$ MeV, and with mean transverse flow velocities $0.33 \leq \langle \beta \rangle \leq 0.39$ over this range of temperatures (219, 220). Thermal fits including resonance decays and transverse flow for SPS data in central S + W collisions are consistent with $T = 160$ MeV and a transverse flow with average velocity $\langle \beta \rangle \approx 0.27$ (221) or with $T = 150$ MeV and $\langle \beta \rangle \approx 0.41$ (222). The central S + S data are compatible with $T = 150$ MeV and with an average velocity $\langle \beta \rangle \approx 0.32$ (77a). These results are consistent with the emitting system being in thermal equilibrium at freeze-out. [The fits presently do not rule out a much higher temperature ($T = 190$ – 230 MeV) combined with the absence of transverse flow in the case of the SPS data (223, 244). A thermal freeze-out at an apparent temperature as high as $T = 230$ MeV is inconsistent with a hadronic picture at freeze-out if the results from the lattice gauge theory on T_c are correct. In this case, hadron emission would have to proceed far off equilibrium, possibly reflecting thermal conditions in a prehadronic phase of the reaction.]

5.3 Chemical Equilibration—Strangeness Production

The assumption of particle emission from a locally thermalized source can be tested by using a thermochemical model to describe the ratios of the various emitted particles. This yields a baryon chemical potential μ_B , a strangeness chemical potential μ_s , and a temperature T at chemical freeze-out that can be compared to the temperatures derived from the particle spectra. Of specific interest are strange particles and antibaryons, whose production is predicted to be enhanced (137, 139) if a chiral phase transition occurs in a dense, baryon-rich system.

An enhancement in the production of strange particles compared with proton-proton and proton-nucleus interactions has been observed and measured for various systems in nucleus-nucleus collisions at the AGS (203) and the SPS (225–229). It should be noted that some increase in the production of strange hadrons, especially kaons and Λ s, in nucleus-nucleus collisions can result from purely hadronic interactions (230–232). However, the measured enhancement in the Λ yield over a large rapidity interval (225) is difficult to describe by a cascade of hadronic interactions. A clear enhancement in the production of $\bar{\Lambda}$, Ξ , Ω , and $\bar{\Omega}$ hyperons (226–228) has been observed at the SPS. To be able to describe this enhancement, severe modifications must be introduced to the hadronic cascade models, invoking precursors of quark-gluon plasma formation such as creation of color ropes (211), breaking of multiple strings (234), or decay of multi-quark droplets (212).

The ratios K^+/K^- , $\bar{\Lambda}/\Lambda$, and \bar{p}/p from the AGS are consistent with an equilibrated hadronic fireball with $\mu_s/T = 0.54 \pm 0.11$ and $\mu_B/T = 3.9 \pm 0.3$ (219, 220, 235). The fit can be improved by including an overall strangeness suppression factor $\gamma_s \approx 0.7$ (235a). The $\bar{\Lambda}/\Lambda$, Ξ/Ξ , Ξ/Λ , and $\Xi/\bar{\Lambda}$ ratios (227) measured at the SPS have been reproduced in an equilibrium hadron

gas description with $\mu_s/T = 0.24 - 0.28$ and $\mu_B/T = 1.05$ (221). The SPS strange particle data have also been described by an equilibrated quark-gluon plasma, with strangeness neutrality ($\mu_s = 0$) and moderate strangeness suppression factor ($\gamma_s \geq 0.5$), which hadronizes and decays instantaneously (141, 224, 236). Further experimental information is necessary to differentiate between the hadron gas and quark-gluon plasma descriptions of the strange particle ratios.

5.4 Two-Particle Correlations

Two-particle interferometric techniques (238) have been used to study the space-time evolution of the colliding systems and to provide information for testing and understanding dynamical models. Pions and kaons will freeze out late in the expansion and will provide information on the system in its later stages. In experiments at SPS energies, the radii extracted from K^+K^+ and K^-K^- interferometry measurements (239) are equal, indicating that the interactions of the kaons with the expanding matter are predominantly $K\pi$ interactions (240). A similar comparison has yet to be made at the AGS, where the central rapidity region has approximately equal numbers of mesons and baryons. At AGS and SPS energies, the radii derived from $\pi\pi$ interferometry are consistently larger than those from KK measurements (239, 241). This has been attributed (241) at the higher energies to effects of resonance decays (242) in addition to the differences in π -hadron and K-hadron interaction cross sections.

The source sizes derived from correlation measurements of each of the particle species provide information on the space-time evolution of the expanding source. The longitudinal and transverse radii measured in central collisions at the SPS are considerably larger than the projectile radius, thus reflecting a large amount of expansion of the system in the final stage before freeze-out (243). A similar, but less pronounced, effect is observed in experiments at the AGS. The longitudinal source radii measured as a function of rapidity (233) can be fit by a boost-invariant longitudinal expansion (244).

At the SPS, a slight decrease in the transverse source radii as a function of increasing transverse momentum has been measured in sulphur-induced collisions (233), and a considerably larger decrease has been observed for the heavy Pb + Pb system (246). The transverse source radii are expected to decrease as a function of increasing transverse momentum in the presence of transverse flow (248, 79a).

In a detailed comparison of a model calculation with the measured data, a correlation is observed between a particle's momentum and position at the time of freeze-out (243). This suggests that kinematic correlations cannot be neglected in the correlation function analysis, and that shadowing and flow effects must be included in interpreting the data.

An overall picture of the source in the late stage of the collision emerges from the $\pi\pi$ correlation measurements. It is one of a pion-emitting source that expands longitudinally, with a weaker transverse expansion that increases with the mass of the colliding system. At SPS energies, the time between the onset of expansion and freeze-out along the longitudinal direction is approximately 5 fm/c, and a small difference between the transverse components is observed, indicating a short duration, not more than 2 fm/c, for particle emission (247). To date, all measurements of the two transverse radius components of the source, which would be distinguishable if a long-lived intermediate phase were to exist, have been identical. Thus, no long-lived intermediate state has yet been observed in the correlation measurements (248).

5.5 *Resonance Matter*

At temperatures and densities just below that of a quark-gluon plasma, nuclear matter is expected to exist in the form of highly excited resonance matter. Microscopic calculations (208, 249) predict that during central collisions at AGS energies, the central rapidity region becomes compressed to high densities, is highly excited, and is baryon-rich (250–252). A significant fraction of the baryons in central collisions will be in excited states (208, 253, 254), forming what might be called baryonic resonance matter. This is consistent with a recent measurement of the Δ resonance population at the time of freeze-out in central collisions at the AGS (255, 256), as well as with results of RQMD, which find that 35% of the final-state nucleons are excited to the Δ resonance at the time of freeze-out. Excitation to higher energies at the SPS, RHIC, and LHC should lead to the formation of highly excited resonance matter. Excitation of higher-lying resonances provides a means of converting energy from the relative motion, thereby increasing the rate of equilibration. Studies of the population of the various resonances in these collisions will provide a test of thermalization and should distinguish features of the collision dynamics between the AGS and SPS energies.

5.6 *Virtual and Real Photons*

An enhancement has been measured in the invariant mass spectrum of muon pairs emitted in central nucleus-nucleus collisions relative to proton-proton and proton-nucleus interactions at 200 A-GeV/c. The observed yields in nucleus-nucleus collisions exceed the contributions from known sources (combinatorial background, Drell-Yan, and open charm and hadronic decays) (257, 258) over the range of invariant masses $0.2 < M < 2.5 \text{ GeV}/c^2$ (up to the onset of the J/ψ for which a suppression is observed) and for all transverse masses, whereas the proton-nucleus data are well described by the same known sources. A large excess is also measured in the low-mass region ($0.2 < M < 1.5 \text{ GeV}/c^2$) for

e^+e^- pairs in S + Au collisions relative to $p + \text{Be}$ and $p + \text{Au}$ interactions at 200 A-GeV/c (259). The spectra for the proton-induced reactions are well-reproduced by e^+e^- pairs from known hadronic sources. The enhanced spectra can be described by assuming medium modifications to the intermediate mass vector meson resonances due to partial chiral symmetry restoration (260).

Direct photon measurements have been made by using nucleus-nucleus collisions in three separate experiments at the SPS, and preliminary results have been reported. No direct photons were observed at the level of approximately 10% systematic error in one experiment (259) and slightly larger systematic error in another (261). A third experiment (262) has reported a 5.8% photon signal over background with a 5% systematic error. Thus, preliminary experimental results are consistent with one another within experimental errors, and a significant direct photon yield has yet to be established.

5.7 J/ψ Suppression

A suppression of J/ψ (263) and ψ' (264) production relative to that of the Drell-Yan continuum has been measured for central collisions in nucleus-nucleus experiments at the SPS. The suppression of the ψ' is observed to be larger than that of the J/ψ in central nucleus-nucleus collisions. Such suppression is expected to result from color screening of the $c\bar{c}$ pair in a deconfined medium (114). It also occurs as a result of final-state interactions in a dense hadronic medium (265). A similar suppression has been seen in J/ψ production in hadron-nucleus interactions (266) and in μ -nucleus interactions (267), lending credence to a hadronic mechanism being responsible for the observed suppression. However, ψ'/ψ ratios have been measured in proton-proton and proton-nucleus interactions and were found to be constant, independent of the nuclear mass of the target (268).

There is presently no unambiguous explanation for the suppression of J/ψ and ψ' in the various interactions in which they have been measured. However, theories describing the suppression of J/ψ and ψ' in nucleus-nucleus collisions require the formation of comoving high-density matter, be it hadronic or deconfined matter. Better knowledge of the various mechanisms for interactions of the J/ψ in hadronic matter and in deconfined matter, as well as for initial- and final-state interactions, is important to an understanding of the suppression.

6. FUTURE MEASUREMENTS

6.1 *Kinematic Probes*

Future experiments will study properties of high baryon density in collisions of the heaviest systems at the AGS and SPS, and high energy density with heavy systems at RHIC and LHC. More information on collective flow at the AGS and

SPS will emerge from the comparison of correlation measurements with single-particle spectra and from calculations using microscopic models. The goal of these investigations will be to better understand the effects of flow on other observables. This will be essential for a knowledge of the space-time evolution of the system and, subsequently, for determining the entropy, temperature, and chemical potentials of the system in the high-density phase. Furthermore, the energy dependence of strangeness and entropy production should be measured in the energy regime from the AGS through the SPS energies, in order to understand the presently observed differences in the strangeness and entropy at the two energies and to search for an onset of a phase transition at moderate-to-high baryon density.

Studies with heavy systems, especially at higher energies, will provide unprecedented energy densities where effects of the quark-gluon plasma and chiral transitions are expected. One of the most interesting aspects of the new experiments will be the use of the increased multiplicities in the heavy systems at SPS and higher energies to extract thermodynamic properties (T , μ_B , S , μ_s , ϵ , etc) of the system on an event-by-event basis (192, 198). This enables categorization of individual events into groups according to thermodynamic properties and could potentially lead to the isolation of events with special properties associated with quark-gluon plasma formation. Ensembles of these events could then be studied in greater detail to determine their particular characteristics.

6.2 *Electromagnetic Probes*

New measurements that use electromagnetic probes to study heavy colliding systems at higher energy densities, at the SPS and at the higher energies of RHIC and the LHC, should provide important results.

The observation of an excess of lepton pairs in the low and intermediate mass region from three different experiments at the SPS requires further experimental and theoretical investigation. There are differences in the measurements that must be understood. Better statistics are needed to be able to understand the dependence of the excess on invariant mass and on collision centrality. For low-mass electron pairs, there appears to be a threshold at $M = 2m_\pi$, a quadratic dependence on rapidity density, and an excess is observed over a broad mass range. These facts suggest that the excess may be due to $\pi^+\pi^-$ pair annihilation. The excess above the ρ , which is similar to the open charm contribution, might be explained by enhanced production of charm.

New results using the heavy systems at the SPS should show an even stronger enhancement of the lepton-pair yields, if the excess seen so far is due to effects of a dense hadronic medium. At RHIC and the LHC, lepton pairs with higher masses, those between the J/ψ and Υ , could be used as a diagnostic tool for the collision dynamics (92). Measurements of the ratios of the ρ , ω , and ϕ

vector mesons will provide information on the time evolution of collisions and, in particular, the lifetime of the fireball.

In measurements of direct photons, better control of experimental conditions is necessary to reduce the systematics to the level required for measuring signals only a few percent above background. Theoretically, it will be important to understand the relationship between the large excess of low-mass electron pairs (virtual photons) and a weak direct photon signal.

Because the transverse mass and momentum distributions of hadrons contain effects that result from resonance production, decays, expansion, and collective flow, it would be extremely interesting to utilize noninteracting probes, such as photons, to measure the temperature of the high-density phase. Clearly, a consistent picture between these results and the temperature derived from the observed particle ratios would be both gratifying and most convincing.

6.3 *Probes of Deconfinement*

Further studies of the relative suppression of J/ψ and ψ' at the SPS in central collisions of very heavy nuclei should provide crucial information on the relative roles of nuclear rescattering, color screening, and deconfinement at the highest energy densities. Measurement of J/ψ and ψ' in $A + p$ interactions using reverse kinematics to measure the J/ψ -hadron rescattering cross sections will be important to understanding the role of rescattering in the breakup of the J/ψ and ψ' . This is an essential step toward isolating the suppression due to screening in a quark-gluon plasma. It will be important to vary the projectile and target masses to determine the A -dependence of the various processes for a complete understanding of the suppression.

At the higher incident energies of RHIC and the LHC, the energy densities will be more than a factor of ten greater than in present measurements at the SPS. Thus, the differences in the J/ψ , ψ' , Υ , and Υ' suppression and in the screening due to quark-gluon plasma formation should be accentuated.

6.4 *Probes of Chiral Symmetry Restoration*

Effects of a high-density nuclear, hadronic, or deconfined medium on the mass and width of the light-vector mesons will be investigated in central collisions of very heavy-ions at the AGS, SPS, RHIC, and LHC. This should provide information on possible resonance mass and width modifications due to the high-density medium and chiral symmetry restoration. Another characteristic of a chiral phase transition would be the observation of abnormal ratios of charged to neutral pions. This will be investigated in event-by-event measurements at higher densities in central collisions of the heavy systems at the SPS, RHIC, and LHC.

6.5 *Other Probes*

Because a significant fraction of the interactions at RHIC and the LHC will be in the perturbative regime, it is important to measure the distributions of the incident partons in nuclei and the nuclear shadowing in collisions of nuclei. Deep-inelastic scattering of leptons from nuclei has provided measurements of the quark momentum distributions in nuclei. However, direct access to the gluon distributions will require measurements of $p + A$ interactions. Comparisons of similar measurements in $A + A$ interactions will provide the understanding of nuclear shadowing necessary to calculate these interactions at the microscopic level.

It would be extremely interesting to measure the total yield of hadrons containing a single c -quark (open charm) at the SPS and at higher energies. Since the initial stages of the collisions at RHIC and LHC are expected to be dominated by gluons, open charm production is expected to be enhanced. Measurement of the amount of open charm will provide information on the initial stages of the collision, prior to formation of a quark-gluon plasma.

Collisions at RHIC and the LHC will exhibit effects of hard scattering of partons. Such QCD hard-scattering processes will result in the production of high- p_T particles and jets which will be measured in experiments at RHIC and the LHC to test the propagation of high- p_T partons in highly excited matter and in a quark-gluon plasma.

New and more sensitive searches for the H-particle (neutral, doubly strange dibaryon) and strangelets have begun at the AGS (270) and SPS (269, 271). These experiments seek either to detect these hypothetical particles or, at a minimum, to set stringent limits on their production cross sections. Such measurements would provide important input into model calculations for the quark structure of nuclei, quark-gluon plasma formation, cosmology, and stellar evolution.

7. SUMMARY

In this review, we described the various signatures proposed for quark-gluon plasma formation and chiral symmetry restoration. These signatures are being pursued vigorously in experiments at the present-day relativistic heavy-ion accelerators, the AGS and SPS, and in the construction of relativistic heavy-ion experiments for RHIC and the LHC. Figure 3 provides an overview of the various signatures described in this review and their expected behavior as the energy density (as measured by the transverse energy density) increases through the critical energy density ϵ_c . Large changes are anticipated as the energy density of the transition is traversed.

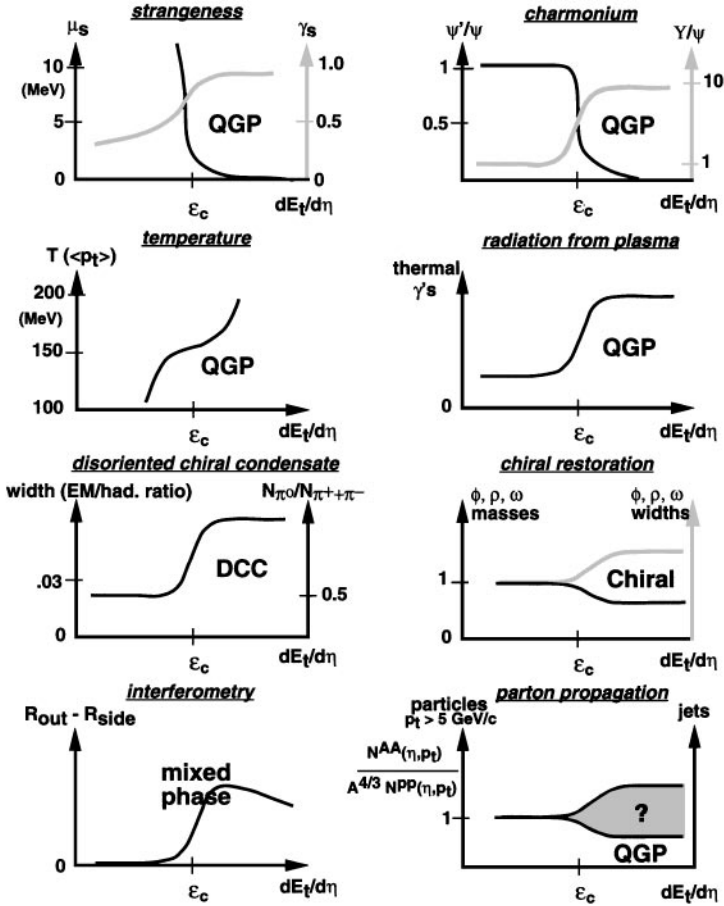
SIGNATURES

Figure 3 Signatures of quark-gluon plasma formation and the chiral phase transition. The expected behavior of the various signatures is plotted as a function of the transverse energy, which is a measure of the energy density, in the region around the critical energy density ϵ_c of the transition. When two curves are drawn, the hatched curve corresponds to the variable described by the hatched ordinate on the right. See text for details.

The searches for signatures of the quark-gluon plasma at the AGS and SPS have provided a valuable initial study of the behavior of these signatures as the critical energy density is approached from below. To date, no unambiguous signal of the quark-gluon plasma or the chiral transition has been seen. However, several experimental results are incompatible with predictions of models based on established knowledge about interacting hadrons. In particular, we note the observation of a substantial enhancement of strange (anti) baryon yields and an increased emission of lepton pairs in the mass region below the ρ -meson. These results may indicate that a quark-gluon plasma or mixed phase is formed in some interactions or regions of interactions at SPS energies, or that hadron masses are substantially reduced during these reactions. It will be up to future investigations to sort this out.

Analysis of the observed hadron spectra and yields has provided evidence that the system, at the moment of breakup, is in a state of local equilibrium not far from the predicted phase boundary between hadron and quark matter, corresponding to $T \approx 160$ MeV and $\mu_B \approx 170$ MeV at the SPS, and $T \approx 130$ MeV and $\mu_B \approx 500$ MeV at the AGS. If the present theory and models are correct and equilibrium is reached at an even earlier stage (before freeze-out) of the reaction, then at a minimum, a quark-hadron mixed phase is formed at the SPS. This spells exceptional promise for experiments at the future heavy-ion colliders, where the full spectrum of quark-gluon plasma signatures can be measured, many on an event-by-event basis.

The success of thermal models in describing the rapidity and transverse momentum spectra and the ratios of various particles has led to a general understanding of the reaction dynamics at these energies. The freeze-out temperatures that have been deduced are in the range $T = 120\text{--}160$ MeV, using best fits to the transverse momentum spectra, which require a moderate amount of transverse flow, $\beta \approx 0.3$. The quark chemical potentials are in the range of $\mu_q = 50\text{--}70$ MeV for the SPS energies and $\mu_q = 150\text{--}200$ MeV for the Brookhaven AGS energies. These measurements can be used to determine the regions of the phase diagram of nuclear matter that are being investigated in these interactions. The resulting points are shown superimposed on a schematic phase diagram of nuclear matter in Figure 4. In studying this diagram, it is important to keep in mind that the freeze-out temperatures are those observed in the particle spectra after interactions cease. In deriving these temperatures, effects of flow and resonance production and decay have been taken into consideration. Temperatures at earlier times during the interaction must have been higher. This has been seen in the results of microscopic, hadronic cascade calculations. The collision evolves from initial nuclear densities and temperatures to higher densities and temperatures prior to expansion and cooling (denoted by

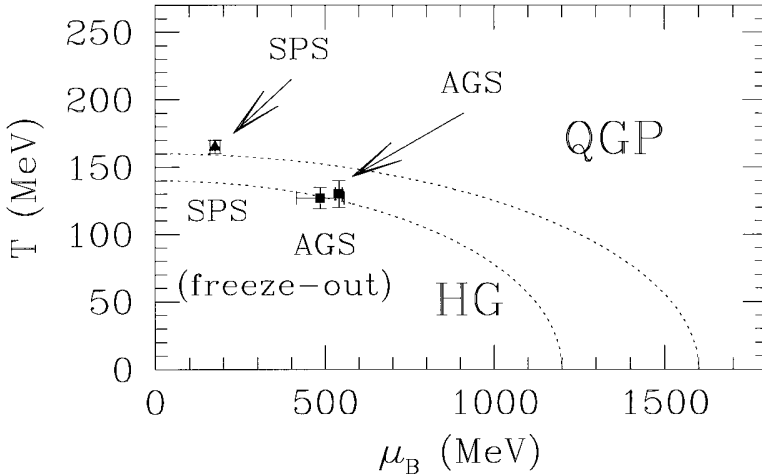


Figure 4 Thermal freeze-out parameters shown in the phase diagram of nuclear matter. The two dashed lines indicate location of the expected phase boundary and its degree of uncertainty. The solid points with error bars show the freeze-out values deduced from AGS and SPS data with flow; the arrows indicate how the freeze-out conditions may be approached during the expansion of the fireball. The horizontal axis shows the baryon chemical potential μ_B , which is a measure of the baryon density.

the arrows for the AGS and SPS measurements) to the final freeze-out values observed in the experiments.

It is the goal of heavy-ion physics to explore the various regions of the phase diagram of nuclear matter (Figure 4) and to map out its properties at these various temperatures and pressures. It is of special interest to relativistic heavy-ion physics to investigate regions of higher temperatures and densities for formation of a quark-gluon plasma and a chiral phase transition. The new relativistic heavy-ion collider experiments will search for the signatures (Figure 3) of these phase transitions, as well as measure observables that reflect variables of the state of the system, in order to determine the characteristics of nuclear matter at high densities.

ACKNOWLEDGMENTS

We thank T Hallman, U Heinz, G Young, and W Zajc for comments on the text. We are indebted to S Nagamiya for the original concept of Figure 3. JWH is grateful for the support of the Alexander von Humboldt Foundation and the hospitality of the Institut für Kernphysik of the Universität Frankfurt.

This work was supported in part by the Director, Office of Energy Research, Division of Nuclear Physics of the Office of High Energy and Nuclear Physics of the US Department of Energy under Contract DE-AC03-76SF00098 and Grant DE-FG05-96ER40945.

Literature Cited

1. Shifman MA. *Annu. Rev. Nucl. Part. Sci.* 33:199 (1983)
2. Pochodzalla J, et al. *Phys. Rev. Lett.* 175:1040 (1995)
3. Collins JC, Perry M. *Phys. Lett.* 34:1353 (1975)
4. Polyakov AM. *Phys. Lett.* 72B:224 (1977)
5. Polonyi J. hep-ph/9509334
6. Pisarski RD, Wilczek F. *Phys. Rev. D* 29:338 (1984)
7. Rajagopal K, Wilczek F. *Nucl. Phys. B* 399:395 (1993)
8. Kolb E, Turner MS. *The Early Universe*. Redwood City, CA: Addison-Wesley (1990)
9. Migdal AB. *ZhETF* 61:2210 (1971); *Nucl. Phys. A* 210:421 (1973)
10. Brown GE, Weise W. *Phys. Rep.* 27C:2 (1976)
11. Lee TD, Wick GC. *Phys. Rev. D* 9:2291 (1974)
12. Bodmer A. *Phys. Rev. D* 4:1601 (1971)
13. Chin SA, Kerman AK. *Phys. Rev. Lett.* 43:1292 (1979)
14. Witten E. *Phys. Rev. D* 30:272 (1984)
15. Farhi E, Jaffe RL. *Phys. Rev. D* 30:2379 (1984)
16. Kaplan DB, Nelson AE. *Phys. Lett.* 175B:57 (1986)
17. Kasuya M, Saito T, Yasue M. *Phys. Rev. D* 47:2153 (1993)
18. Gilson EP, Jaffe RL. *Phys. Rev. Lett.* 71:332 (1993)
19. Madsen J. *Phys. Rev. Lett.* 70:391 (1993); *Phys. Rev. D* 47:5156 (1993)
20. Desai MS, Crawford HJ, Shaw GL. *Phys. Rev. D* 47:2063 (1993)
21. Liu H, Shaw GL. *Phys. Rev. D* 30:1137 (1984)
22. Greiner C, Koch P, Stöcker H. *Phys. Rev. Lett.* 58:1109 (1987)
23. Greiner C, Stöcker H. *Phys. Rev. D* 44:3517 (1991)
24. Crawford HJ, Desai MS, Shaw GL. *Phys. Rev. D* 45:857 (1992)
25. Madsen J. *Phys. Rev. Lett.* 61:2909 (1988)
26. Wilson K. *Phys. Rev. D* 10:2445 (1974)
27. Creutz M. *Quarks, Gluons and Lattices*. Cambridge: Cambridge Univ. Press. (1983)
28. Blum T, Kärkkäinen L, Toussaint D, Gottlieb S. *Phys. Rev. D* 51:5153 (1995)
29. Boyd G, et al. *Phys. Rev. Lett.* 75:4169 (1995); *Phys. Lett.* 349B:170 (1995)
- 29a. Asakawa M, Hatsuda T. Preprint (hep-ph/9508360)
30. Biró T, Levai P, Müller B. *Phys. Rev. D* 42:3078 (1990)
31. Peshier A, Kämpfer B, Pavlenko OP, Soff G. *Phys. Lett.* 337B:235 (1994)
32. Baym G, Chin SA. *Phys. Lett.* 62B:241 (1976); Chin SA. *Phys. Lett.* 78B:552 (1978)
33. Friedman B, McLerran L. *Phys. Rev. D* 17:1109 (1978)
34. Shuryak EV. *Phys. Rep.* 61:71 (1980)
35. Arnold P, Zhai CX. *Phys. Rev. D* 51:1906 (1995); Zhai CX, Kastening B. *Phys. Rev. D* 52:7232 (1995)
36. Klimov W. *Sov. Phys. JETP* 55:199 (1982)
37. Weldon HA. *Phys. Rev. D* 26:1394 (1982)
38. Biró TS, Gong C, Müller B. *Phys. Rev. D* 52:1260 (1995)
39. Hwa RC, Kajantie K. *Phys. Rev. Lett.* 56:696 (1986)
40. Blaizot JP, Mueller AH. *Nucl. Phys. B* 289:847 (1987)
41. Anishetty R, Koehler P, McLerran L. *Phys. Rev. D* 22:2793 (1980)
42. Bialas A, Czyż W. *Phys. Rev. D* 31:198 (1985)
43. Kajantie K, Matsui T. *Phys. Lett.* 164B:373 (1985)
44. Wang XN, Gyulassy M. *Phys. Rev. D* 44:3501 (1991); *Phys. Rev. D* 45:844 (1992); *Comp. Phys. Comm.* 83:307 (1994)
45. Geiger K, Müller B. *Nucl. Phys. B* 369:600 (1992)
46. Geiger K. *Phys. Rep.* 258:237 (1995)
47. Eskola KJ, Wang XN. *Phys. Rev. D* 49:1284 (1994)
48. Shuryak E. *Phys. Rev. Lett.* 68:3270 (1992)
49. Biró TS, et al. *Phys. Rev. C* 48:1275 (1993)

50. Geiger K, Kapusta JI. *Phys. Rev. D* 47:4905 (1993)
51. Xiong L, Shuryak EV. *Phys. Rev. C* 49:2207 (1994)
52. Gyulassy M, Rischke DH. Private communication
53. Bjorken JD. *Phys. Rev. D* 27:140 (1983)
54. Blaizot JP, Ollitrault JY. *Quark-Gluon Plasma*, ed. RC Hwa. Singapore: World Sci. 393 pp. (1991)
55. Hung CM, Shuryak EV. *Phys. Rev. Lett.* 75:4003 (1995)
56. Rischke DH, Gyulassy M. *Nucl. Phys. A* 597:701 (1996)
57. Pratt S. *Phys. Rev. Lett.* 53:1219 (1984); *Phys. Rev. D* 33:1314 (1986)
58. Bertsch G, Gong M, Tohyama M. *Phys. Rev. C* 37:1896 (1988); Bertsch GF. *Nucl. Phys. A* 498:173c (1989)
59. Gavin S. *Nucl. Phys. A* 544:459 (1992)
60. Haglin K, Pratt S. *Phys. Lett. B* 328:255 (1994)
61. Kajantie K, McLerran L. *Annu. Rev. Nucl. Part. Sci.* 37:293 (1987)
62. Bernard V. *Quark-Gluon Plasma Signatures*. Paris: Editions Frontières (1990)
63. Singh CP. *Phys. Rep.* 236:147 (1993)
64. Müller B. *Rep. Prog. Phys.* 58:611 (1995)
65. van Hove L. *Phys. Lett.* 118B:138 (1982); *Z. Phys. C* 21:93 (1983)
66. von Gersdorff H, McLerran L, Kataja M, Ruuskanen PV. *Phys. Rev. D* 34:794 (1986); Kataja M, Ruuskanen PV, McLerran L, von Gersdorff H. *Phys. Rev.* 34:3755 (1986)
67. Kataja M, Ruuskanen PV, Letessier J, Tounsi A. *Z. Phys. C* 55:153 (1992)
- 67a. Schnedermann E, Heinz U. *Z. Phys. C* 48:525 (1990)
68. Blaizot JP, Ollitrault JY. *Nucl. Phys. A* 458:745 (1986)
69. Gyulassy M, Kajantie K, Kurki-Suonio H, McLerran L. *Nucl. Phys. B* 237:477 (1984)
70. Pisarski RD. *Phys. Lett.* 110B:155 (1982)
71. Bochkarev AI, Shaposhnikov ME. *Phys. Lett.* 145B:276 (1984); *Nucl. Phys. B* 268:220 (1986); *Z. Phys. C* 36:267 (1987)
72. Dosch HG, Narison S. *Phys. Lett.* 203B:155 (1988)
73. Furnstahl RJ, Hatsuda T, Lee SH. *Phys. Rev. D* 42:1744 (1990)
74. Gale C, Kapusta J. *Nucl. Phys. B* 357:65 (1991)
75. Barz HW, Csernai LP, Kämpfer B, Lukács B. *Phys. Rev. D* 32:115 (1985)
76. Seibert D. *Phys. Rev. D* 32:2812 (1987); *Phys. Rev. D* 35:2013 (1987)
77. Bilić N, Cleymans J, Suhonen E, van Oertzen DW. *Phys. Lett.* 311B:266 (1993)
- 77a. Schnedermann E, Sollfrank J, Heinz U. *Phys. Rev. C* 48:2462 (1993)
78. Csörgö T. *Phys. Lett.* 347B:354 (1994).
79. Csörgö T, Lörstad B. *Nucl. Phys. A* 590:465 (1995)
- 79a. Wiedemann UA, Scotto P, Heinz U. *Phys. Rev. C* 53:918 (1996)
80. Chu MC, Gardner S, Matsui T, Seki R. *Phys. Rev. C* 50:3079 (1994)
81. Feinberg EL. *Nuovo Cim.* 34A:391 (1976)
82. Shuryak EV. *Phys. Lett.* 78B:150 (1978)
83. Domokos G, Goldman JI. *Phys. Rev. D* 23:203 (1981)
84. Kajantie K, Miettinen HI. 1981 *Z. Phys. C* 9:341 (1981); *Z. Phys. C* 14:357 (1982)
85. Chin SA. *Phys. Lett.* 119B:51 (1982)
86. Hwa R, Kajantie K. *Phys. Rev. D* 32:1109 (1985)
87. Cleymans J, Fingberg J. *Phys. Lett.* 168B:405 (1986); Cleymans J, Fingberg J, Redlich K. *Phys. Rev. D* 35:2153 (1987)
88. Kajantie K, Kataja M, McLerran L, Ruuskanen PV. *Phys. Rev. D* 34:811 (1986); Kajantie K, Kapusta J, McLerran L, Mekjian A. *Phys. Rev. D* 34:2746 (1986)
89. Cleymans J, Redlich K, Satz H. *Z. Phys. C* 52:517 (1991)
90. Gale C, Lichard P. *Phys. Rev. D* 49:3338 (1994); Song C, Ko CM, Gale C. *Phys. Rev. D* 50:R1827 (1994)
91. Ruuskanen PV. *Nucl. Phys. A* 525:255c (1991); *ibid.* A544:169c (1992)
92. Kapusta J, McLerran L, Srivastava DK. *Phys. Lett.* 283B:145 (1992)
93. Geiger K, Kapusta JI. *Phys. Rev. Lett.* 70:1920 (1993)
94. Shuryak EL, Xiong L. *Phys. Rev.* 70:2241 (1993)
95. Kämpfer B, Pavlenko OP. *Phys. Lett.* 289B:127 (1992); *Nucl. Phys. A* 566:351c (1994)
96. Strickland MT. *Phys. Lett.* 331B:245 (1994)
97. Vogt R, Jacak BV, McGaughey PL, Ruuskanen PV. *Phys. Rev. D* 49:3345 (1994)
98. Lin Z, Gyulassy M. *Phys. Rev. C* 51:2177 (1995); *ibid.* Erratum. C52:440 (1995)
99. Levai P, Müller B, Wang XN. *Phys. Rev. C* 51:3326 (1995)

100. Sarcevic I, Valerio P. *Phys. Lett.* 338B:416 (1994); *Phys. Rev. C* 51:1433 (1995)
- 100a. McGaughey PL, et al. *Int. J. Mod. Phys. A* 10:2999 (1995)
101. Siemens PJ, Chin SA. *Phys. Rev. Lett.* 55:1266 (1985)
102. Seibert D. *Phys. Rev. Lett.* 68:1476 (1992); Seibert D, Mishra VK, Fai G. *Phys. Rev. C* 46:330 (1992)
103. Gale C, Kapusta J. *Phys. Rev. C* 35:2107 (1987)
104. Karsch F, Redlich K, Turko L. *Z. Phys. C* 60:519 (1995)
105. Heinz U, Lee KS. *Phys. Lett.* 259B:162 (1991)
106. Kapusta J, Lichard P, Seibert D. *Phys. Rev. D* 44:2774 (1991); *ibid.* Erratum. 47:4171 (1993)
107. Xiong L, Shuryak E, Brown GE. *Phys. Rev. D* 46:3798 (1992)
108. Baier R, Nakkagawa H, Niegawa A, Redlich K. *Z. Phys. C* 53:433 (1992); *Phys. Rev. D* 45:4323 (1992)
109. Srivastava DK, Sinha B, Gyulassy M, Wang XN. *Phys. Lett.* 276B:285 (1992)
110. Chakrabarty S, et al. *Phys. Rev. D* 46:3802 (1992)
111. Seibert D. *Z. Phys. C* 58:307 (1993)
112. Alam J, Srivastava DK, Sinha B, Basu DN. *Phys. Rev. D* 48:1117 (1993)
113. Neumann JJ, Seibert D, Fai G. *Phys. Rev. C* 51:1460 (1995)
114. Matsui T, Satz H. *Phys. Lett.* 178B:416 (1986)
115. Karsch F, Mehr MT, Satz H. *Z. Phys. C* 37:617 (1988)
116. DeGrand TA, DeTar CE. *Phys. Rev. D* 34:2469 (1986)
117. Kanaya K, Satz H. *Phys. Rev. D* 34:3193 (1986)
118. Karsch F, Wyld HW. *Phys. Lett.* 213B:505 (1988)
119. Blaschke D. *Nucl. Phys. A* 525:269c (1991)
120. Karsch F, Satz H. *Z. Phys. C* 51:209 (1991)
121. Černý V, et al. *Z. Phys. C* 46:481 (1990)
122. Hüfner J, Povh P, Gardner S. *Phys. Lett.* 238B:103 (1990)
123. Cleymans J, Thews RL. *Z. Phys. C* 45:391 (1990)
124. Blaizot JP, Ollitrault JY. *Phys. Lett.* 199B:499 (1987)
125. Karsch F, Petronzio R. *Phys. Lett.* 212B:255 (1988)
126. Gaździcki M, Mrówczyński S. *Z. Phys. C* 49:546 (1991)
127. Lietava R. *Z. Phys. C* 50:107 (1991)
128. Gavin S, Gyulassy M, Jackson A. *Phys. Lett.* 207B:257 (1988)
129. Vogt R, Prakash M, Koch P, Hansson TH. *Phys. Lett.* 208B:263 (1988)
130. Martins K, Blaschke D, Quack E. *Phys. Rev. C* 51:2723 (1995)
- 130a. Wittmann R, Heinz U. *Z. Phys. C* 59:77 (1993)
131. Kharzeev D, Satz H. *Phys. Lett.* B366:316 (1996)
132. Gupta S, Satz H. *Phys. Lett.* 283B:439 (1992)
133. Vogt R, Brodsky SJ, Hoyer P. *Nucl. Phys. B* 383:643 (1992)
134. Doncheski MA, Gay Ducati MB, Halzen F. *Phys. Rev. D* 49:1231 (1994)
135. Gavin S, Satz H, Thews RL, Vogt R. *Z. Phys. C* 61:351 (1994); Gavin S. *Nucl. Phys. A* 566:383c (1994)
136. Bailly JP, et al. *Phys. Lett.* 195B:609 (1987)
137. Rafelski J, Müller B. *Phys. Rev. Lett.* 48:1066 (1982); *ibid.* Erratum. 56:2334 (1986)
138. Rafelski J. *Phys. Rep.* 88:331 (1982)
139. Koch P, Müller B, Rafelski J. *Phys. Rep.* 142:167 (1986)
140. Heinz U. *Nucl. Phys. A* 566:205c (1994)
141. Letessier J, Tounsi A, Rafelski J. *Phys. Lett.* 292B:417 (1992)
142. Letessier J, Rafelski J, Tounsi A. *Phys. Lett.* 321B:394 (1994)
143. Barz HW, Friman GL, Knoll J, Schulz H. *Nucl. Phys. A* 484:661 (1988); *Nucl. Phys. A* 519:831 (1990); *Phys. Lett.* 254B:315 (1991)
144. Baranov SP, Fil'kov LV. *Z. Phys. C* 57:149 (1993)
145. Bjorken JD. *Acta Phys. Polon. B* 23:637 (1992)
146. Lattes CMG, Fujimoto Y, Hasegawa S. *Phys. Rep.* 65:151 (1980)
147. Lam CS, Lo SY. *Phys. Rev. Lett.* 52:1184 (1984); *Phys. Rev. D* 33:1336 (1986)
148. Pratt S. *Phys. Lett.* 301B:159 (1993); Pratt S, Zelevinsky V. *Phys. Rev. Lett.* 72:816 (1994)
149. Anselm AA, Ryskin MG. *Phys. Lett.* 266B:482 (1989)
150. Blaizot JP, Krzywicki A. *Phys. Rev. D* 46:246 (1992)
151. Kowalski KL, Taylor CC. Preprint CWRUTH-92-6
152. Rajagopal K, Wilczek F. *Nucl. Phys. B* 404:577 (1993)
153. Gavin S, Gocksch A, Pisarski RD. *Phys. Rev. Lett.* 72:2143 (1994)
154. Cooper F, Kluger Y, Mottola E, Paz JP. *Phys. Rev. D* 51:2377 (1995)

155. Asakawa Y, Huang Z, Wang XN. *Phys. Rev. Lett.* 74:3126 (1995)
156. Boyanovsky D, Lee D-S, Singh A. *Phys. Rev. D* 48:800 (1993); Boyanovsky D, deVega HJ, Holman R. *Phys. Rev. D* 51:734 (1995)
157. Bedaque P, Das A. *Mod. Phys. Lett.* 8A:3151 (1993)
158. Gavin S, Müller B. *Phys. Lett.* 329B:486 (1994)
159. Cohen TD, Banerjee MK, Nielsen M, Jin XM. *Phys. Lett.* 333B:166 (1994)
160. Greiner C, Gong C, Müller B. *Phys. Lett.* 316B:226 (1993)
161. DeGrand TA. *Phys. Rev. D* 30:2001 (1984)
162. Ellis J, Heinz U, Kowalski KL. *Phys. Lett.* 233B:223 (1989)
163. Kapusta JJ, Srivastava A. *Phys. Rev. D* 50:5379 (1994)
164. Barz HW, et al. *Phys. Lett.* 265B:219 (1991)
165. Aouissat Z, Chanfray G, Schuck P, Welke G. Z. *Phys. A* 340:347 (1991)
166. Asakawa M, Ko CM, Lévai P, Qiu XJ. *Phys. Rev. C* 46:1159 (1992)
167. Herrmann M, Friman BL, Nörenberg W. Z. *Phys. A* 343:119 (1992)
168. Hatsuda T, Koike Y, Lee SH. *Nucl. Phys. B* 394:221 (1993)
169. Haglin KL, Gale C. *Nucl. Phys. B* 421:613 (1994)
170. Lissauer D, Shuryak EV. *Phys. Lett.* 253B:15 (1991)
171. Bi PZ, Rafelski J. *Phys. Lett.* 262B:485 (1991)
172. Asakawa M, Ko CM. *Phys. Lett.* 322B:33 (1994); Ko CM, Seibert D. *Phys. Rev. C* 49:2198 (1994)
173. Bjorken JD. Fermilab publication 82/59
174. Svetitsky B. *Phys. Rev. D* 37:2484 (1988)
175. Thoma MH, Gyulassy M. *Nucl. Phys. B* 351:491 (1991); Braaten E, Thoma MH. *Phys. Rev. D* 44:R2625 (1991)
176. Mrówczyński S. *Phys. Lett.* 269B:383 (1991)
177. Koike Y, Matsui T. *Phys. Rev. D* 45:3237 (1992)
178. Migdal AB. *Sov. Phys. JETP* 5:527 (1957)
179. Gyulassy M, Wang XN. *Nucl. Phys. B* 420:583 (1994)
180. Baier R, Dokshitzer Yu L, Peigné S, Schiff D. *Phys. Lett.* 345B:277 (1995)
181. Appel DA. *Phys. Rev. D* 33:717 (1986)
182. Blaizot JP, McLerran L. *Phys. Rev. D* 34:2739 (1986)
- 182a. Rammerstorfer M, Heinz U. *Phys. Rev. D* 41:306 (1990)
183. Pan J, Gale C. *Phys. Rev. D* 50:3235 (1994)
184. Corcoran MD, et al. *Phys. Lett.* 259B:209 (1991)
- 184a. Gupta S. *Phys. Lett.* B347:381 (1995)
185. Walenta AH. *Nucl. Instr. Meth.* 161:435 (1979); Allison WWM, Cobb JH. *Annu. Rev. Nucl. Part. Sci.* 30:253 (1980)
186. *Conceptual Design Report of the Relativistic Heavy Ion Collider*. Brookhaven Natl. Lab. Rep. BNL-52195 (1989)
187. Harris J, et al. *Nucl. Phys. A* 566:277c (1994); Nagamiya S. *Nucl. Phys. A* 566:287c (1994); Videbaek F, et al. *Nucl. Phys. A* 566:299c (1994); Wyslouch B. *Nucl. Phys. A* 566:305c (1994)
188. Schukraft J, et al. *Nucl. Phys. A* 566:311c (1994)
189. Aid S, et al. *Phys. Lett.* 354B:494 (1995); *Nucl. Phys. B* 449:3 (1995)
190. Lutz G, Schwarz AS. *Annu. Rev. Nucl. Part. Sci.* 45:295 (1995)
191. Blum W, Rolandi L. *Particle Detection with Drift Chambers*, ed. Bonaudi F, Fabjan CW. Berlin: Springer-Verlag (1994)
192. Stock R. *Hot Hadronic Matter, Theory and Experiment*, ed. J Letessier, HH Gutbrod, J Rafelski. New York: Plenum. 507 pp. (1995)
193. Fabjan C. *Experimental Techniques in High Energy Physics*, ed. T Ferbel. Menlo Park, CA: Addison-Wesley. 257 pp. (1987)
194. Ellis N, Virdee TS. *Annu. Rev. Nucl. Part. Sci.* 44:609 (1994)
195. Kierstaed JA, et al. Brookhaven Natl. Lab. Rep. BNL-52321. 215 pp. (1991)
196. *PHOBOS Conceptual Design Report* (1993); Wyslouch B. *Nucl. Phys. A* 566:305c (1994)
197. *BRAHMS Conceptual Design Report* (1994); Videbaek F, et al. *Nucl. Phys. A* 566:299c (1994)
198. *STAR Conceptual Design Report*. Lawrence Berkeley Lab. Rep. PUB-5347 (1992); Harris J, et al. *Nucl. Phys. A* 566:277c (1994)
199. *ALICE Technical Proposal*. CERN/LHCC 95-71 (1995); Schukraft J, et al. *Nucl. Phys. A* 566:311c (1994)
200. *PHENIX Conceptual Design Report* (1993); Nagamiya S. *Nucl. Phys. A* 566:287c (1994)
201. Stachel J, Young GR. *Annu. Rev. Nucl. Part. Sci.* 42:537 (1992)
202. Blobel V, et al. *Nucl. Phys. B* 69:454 (1974)
203. Abbott T, et al. *Phys. Rev. C* 50:1024 (1994)

204. Barrette J, et al. *Phys. Rev. C* 50:3047 (1994)
205. Baechler J, et al. *Phys. Rev. Lett.* 72:1419 (1994)
206. Videbaek F, et al. *Nucl. Phys. A* 590:249c (1995)
207. Dodd J, et al. *Proc. XXV Int. Symp. Multiparticle Dynamics, Stara Lesnia, Slovakia* (1995); Seyboth P, et al. *ibid*
208. Pang Y, Schlagel TJ, Kahana SH. *Phys. Rev. Lett.* 68:2743 (1992)
209. Werner K. *Phys. Rep.* 232:87 (1993)
210. Anderson B, et al. *Nucl. Phys. B* 281:289 (1987); *Comp. Phys. Comm.* 43:387 (1987); Sjostrand T. *Comp. Phys. Comm.* 82:74 (1994)
211. Sorge H, Berenguer M, Stöcker H, Greiner W. *Phys. Lett.* 289B:6 (1992)
212. Aichelin J, Werner K. *Phys. Lett.* 300B:158 (1993)
213. Barrette J, et al. *Phys. Rev. Lett.* 70:2996 (1993)
214. Barrette J, et al. *Nucl. Phys. A* 566:411c (1994)
215. Alber T, et al. *Phys. Rev. Lett.* 74:1303 (1995)
216. Baechler J, et al. *Z. Phys. C* 52:239 (1991)
217. Gustafsson H-A, et al. *Phys. Rev. Lett.* 52:1590 (1984); Renfordt RE, et al. *Phys. Rev. Lett.* 53:793 (1984)
218. Barrette J, et al. *Phys. Rev. Lett.* 73:2532 (1994)
219. Braun-Munzinger P, Stachel J, Wessels JP, Xu N. *Phys. Lett.* 344B:43 (1995)
220. Letessier J, Rafelski J, Tounsi A. *Phys. Lett.* 328B:499 (1994)
221. Braun-Munzinger P, Stachel J, Wessels JP, Xu N. *Phys. Lett.* 365B:1 (1996)
222. Letessier J, et al. *Phys. Rev. D* 51:3408 (1995)
223. Rafelski J. *Phys. Lett.* 262B:333 (1991)
224. Sollfrank M, Gazdzicki M, Heinz U, Rafelski J. *Z. Phys. C* 61:659 (1994)
225. Alber T, et al. *Z. Phys. C* 64:195 (1994)
226. Anderson E, et al. *Phys. Lett.* 294B:127 (1992); *Phys. Lett.* 327B:433 (1994)
227. Abatzis S, et al. *Nucl. Phys. A* 566:499c (1994); *ibid.* 566:491c (1994); *ibid.* 566:225c (1994); *Phys. Lett.* 316B:615 (1993); DiBari D, et al. *Nucl. Phys. A* 590:307c (1995)
228. Kinson JB, et al. *Nucl. Phys. A* 590:317c (1995)
229. Gazdzicki M, et al. *Nucl. Phys. A* 590:197c (1995)
230. Matsui T, Svetitsky B, McLerran LD. *Phys. Rev. D* 34:2047 (1986)
231. Lee KS, Rhoades-Brown M, Heinz U. *Phys. Rev. C* 37:1452 (1988)
232. Mattiello R, Sorge H, Stöcker H, Greiner W. *Phys. Rev. Lett.* 63:1459 (1989)
233. Alber T, et al. *Z. Phys. C* 66:77 (1995)
234. Werner K, Aichelin J. *Phys. Lett.* B308:372 (1993)
235. Rafelski J, Danos M. *Phys. Rev. C* 50:1684 (1994)
- 235a. Sollfrank J, Heinz U. *Quark-Gluon Plasma 2*, ed. R Hwa. Singapore: World Scientific. 555 pp. (1995)
236. Letessier J, et al. *Phys. Rev. Lett.* 70:3530 (1993)
237. Deleted in proof
238. Zajc WA. *Particle Production in Highly Excited Matter*, ed. HH Gutbrod, J Rafelski. New York: Plenum. 435 pp. (1993)
239. Beker H, et al. *Z. Phys. C* 64:209 (1994); *Phys. Rev. Lett.* 74:3340 (1995)
240. Murray M, et al. *Nucl. Phys. A* 566:589c (1994)
241. Sullivan JP, et al. *Phys. Rev. Lett.* 70:3000 (1993)
242. Gyulassy M, Padula S. *Phys. Lett.* 217B:181 (1988)
243. Jacak B, et al. *Nucl. Phys. A* 590:215c (1995); Fields DE, et al. LA-UR-95-666 (1995)
244. Makhlin AN, Sinyukov YM. *Z. Phys. C* 39:69 (1988)
245. Alber T, et al. *Nucl. Phys. A* 590:453c (1995)
246. Pratt S. *Phys. Rev. D* 33:1314 (1986); *Phys. Rev. Lett.* 53:1219 (1984)
247. Ferenc D, et al. *Nucl. Phys. A* 544:531c (1992); Röhrich D, et al. *Nucl. Phys. A* 566:35c (1994)
248. Alber T, et al. *Phys. Rev. Lett.* 74:1303 (1995); Jacak BV, et al. *Nucl. Phys. A* 590:215c (1995); Cianciolo V, et al. *Nucl. Phys. A* 590:459c (1995); Miskowiec D, et al. *Nucl. Phys. A* 590:473c (1995)
249. Sorge H, et al. *Phys. Rev. Lett.* 86:286 (1992)
250. Stöcker H, Greiner W. *Phys. Rep.* 137:227 (1986)
251. Sorge H, et al. *Phys. Lett.* 243B:7 (1990)
252. Schlagel TJ, Kahana SH, Pang Y. *Phys. Rev. Lett.* 69:3290 (1992)
253. Sorge H, et al. *Phys. Lett.* 251B:37 (1991)
254. Hofmann M, et al. *Nucl. Phys. A* 566:15c (1994)
255. Hemmick T, et al. *Nucl. Phys. A* 566:379c (1994)
256. Barrette J, et al. *Phys. Lett.* 351B:93 (1995)

257. Lourenco C, et al. *Proc. 5th Conf. Intersections Between Part. and Nucl. Phys., St. Petersburg, FL* (1994)
258. Masera M, et al. *Nucl. Phys. A* 590:93c (1995)
259. Agakichiev G, et al. *Phys. Rev. Lett.* 75:1272 (1995)
260. Li GQ, Ko CM, Brown GE. Texas A and M preprint (1996)
261. Akesson T, et al. *Z. Phys. C* 46:369 (1990)
262. Albrecht R, et al. CERN PPE/95-186 preprint (1995)
263. Baglin C, et al. *Phys. Lett.* 220B:471 (1989); *ibid.* 251B:465 (1990); *ibid.* 262B:362 (1991); *ibid.* 268B:453 (1991); *ibid.* 270B:105 (1991)
264. Abreu MC, et al. *Nucl. Phys. A* 566:77c (1994); *ibid.* 566:371c (1994); *ibid.* 590:117c (1995)
265. Gavin S, Satz H, Thews RL, Vogt R. *Z. Phys. C* 61:351 (1994); Gavin S. *Nucl. Phys. A* 566:383c (1994)
266. Alde DM, et al. *Phys. Rev. Lett.* 66:133 (1991)
267. Amandruz P, et al. CERN-PPE-91-198 preprint (1991)
268. Ramos S, et al. *Nucl. Phys. A* 590:117c (1995)
269. Dittus F, et al. *Nucl. Phys. A* 590:347c (1995)
270. Kumar S, et al. *Nucl. Phys. A* 590:29c (1995)
271. Borer K, et al. *Phys. Rev. Lett.* 72:1415 (1994)